IMMUNOLOGY

B7-H3×4-1BB bispecific antibody augments antitumor immunity by enhancing terminally differentiated CD8$^+$ tumor-infiltrating lymphocytes

Gihoon You[1]*, Yangsoon Lee[2]*, Yeon-Woo Kang[1], Han Wook Park[1], Kyeongsu Park[2], Hyekang Kim[1], Young-Min Kim[1], Sora Kim[1], Ji-Hae Kim[3], Dain Moon[1], Hyejin Chung[2], Wonjun Son[2], Ui-jung Jung[2], Eunyoung Park[2], Shinai Lee[2], Yong-Gyu Son[2], Jaehyun Eom[2], Jonghwa Won[2], Yunji Park[1], Jaeho Jung[2†], Seung-Woo Lee[1,3†]

Cancer immunotherapy with 4-1BB agonists has limited further clinical development because of dose-limiting toxicity. Here, we developed a bispecific antibody (bsAb; B7-H3×4-1BB), targeting human B7-H3 (hB7-H3) and mouse or human 4-1BB, to restrict the 4-1BB stimulation in tumors. B7-H3×m4-1BB elicited a 4-1BB–dependent antitumor response in hB7-H3–overexpressing tumor models without systemic toxicity. BsAb primarily targets CD8 T cells in the tumor and increases their proliferation and cytokine production. Among the CD8 T cell population in the tumor, 4-1BB is solely expressed on PD-1$^+$Tim-3$^+$ "terminally differentiated" subset, and bsAb potentiates these cells for eliminating the tumor. Furthermore, the combination of bsAb and PD-1 blockade synergistically inhibits tumor growth accompanied by further increasing terminally differentiated CD8 T cells. B7-H3×h4-1BB also shows antitumor activity in h4-1BB–expressing mice. Our data suggest that B7-H3×4-1BB is an effective and safe therapeutic agent against B7-H3–positive cancers as monotherapy and combination therapy with PD-1 blockade.

INTRODUCTION

Modulation of cosignaling receptors on immune cells is a promising approach for immunotherapy of cancer. Immune checkpoint inhibitors, which block coinhibitory signaling pathways such as the cytotoxic T lymphocyte–associated antigen 4 (CTLA-4) and programmed cell death 1 (PD-1)/programmed cell death ligand 1 (PD-L1) pathways, have been clinically approved for the treatment of a broad range of cancers. Because the response rate to immune checkpoint blockades (ICBs) varies among patients and cancer types, there is an unmet need for innovative immunotherapies with better efficacy (*1*–*3*).

4-1BB (CD137, *tnfrsf9*) is a costimulatory receptor that belongs to the tumor necrosis factor (TNF) receptor superfamily. 4-1BB is broadly expressed on immune cells, including activated T cells, regulatory T (T_{reg}) cells, natural killer (NK) cells, B cells, dendritic cells (DCs), and nonhematopoietic cells such as activated endothelial cells. The binding of 4-1BB with 4-1BB ligand (4-1BBL; *tnfsf9*), which is expressed on antigen-presenting cells, induces clustering of 4-1BB and activates 4-1BB signaling (*4*, *5*). 4-1BB–mediated costimulation of T cells enhances proliferation, cytotoxicity, and cytokine secretion and protects them from activation-induced cell death (*6*–*8*). The expression of 4-1BB reflects specific T cell receptor (TCR)–triggered activation resulting from antigen challenges, including tumors. Because 4-1BB–expressing tumor-infiltrating CD8 T cells are believed to be tumor-reactive T cells (*9*, *10*), 4-1BB is a promising target for cancer immunotherapy by targeting tumor-reactive T cells.

The therapeutic efficacy of 4-1BB agonists has been demonstrated in a variety of preclinical tumor models over the past few decades (*11*), and the preclinical data have led to the entry of two anti–human 4-1BB (h4-1BB)–agonistic monoclonal antibodies (mAbs) into clinical trials, including urelumab [BMS-663513, human immunoglobulin G4 (IgG4)] and utomilumab (PF-05082566, human IgG2). These two antibodies showed several limitations in the clinical trials: Urelumab caused severe dose-dependent hepatotoxicity despite its antitumor efficacy, while utomilumab had relatively low efficacy but with a better safety profile (*7*, *12*). Similar to the data from the clinical trials using urelumab, systemic administration of 4-1BB agonistic mAbs was shown to cause on-target off-tumor immune-related adversary effects (irAEs) in normal mice (*13*, *14*). 4-1BB agonistic mAbs induce splenomegaly followed by extramedullary hematopoiesis and increase CD8 T cell infiltration into the liver and the level of liver enzymes in the serum, which are indicators of liver toxicity. Also, they induce bone marrow (BM) failure, including defects in the development of B and NK cells (*15*). The induction of irAE primarily requires CD8 T cells and the production of cytokines such as TNF-α, interferon-γ (IFN-γ), and IFN-α (*13*). Several approaches have been used to reduce off-tumor toxicity and retain the potent antitumor activity during the development of 4-1BB agonists, including modification of the Fc region of 4-1BB agonistic mAb (*16*) and the addition of tumor-targeting moieties to the 4-1BB agonist to generate bispecifics (*17*–*19*). Tumor-associated antigens (TAAs), such as epidermal growth factor receptor (EGFR) (*17*), fibroblast activation protein (FAP), CD19 (*18*), and human EGFR 2 (HER2) (*19*), have been targeted to develop 4-1BB bispecifics. While these proteins are overexpressed on tumors, their expression in healthy tissues necessitates the identification of other specific cell surface molecules to target 4-1BB agonists to the tumors.

Upon chronic antigen stimulation, such as during chronic viral infection and in tumors, CD8 T cells differentiate into two distinct

[1]Division of Integrative Biosciences and Biotechnology, Pohang University of Science and Technology (POSTECH), Pohang, Republic of Korea. [2]ABL Bio Inc., Seongnam, Republic of Korea. [3]Department of Life Sciences, POSTECH, Pohang, Republic of Korea.
*These authors contributed equally to this work.
†Corresponding author. Email: sw_lee@postech.ac.kr (S.-W.L.); jaeho.jung@ablbio.com (J.J.)

populations: transcription factor T cell factor 1 (TCF1)$^+$ stem-like and T cell immunoglobulin and mucin domain–containing protein 3 (Tim-3)$^+$ terminally differentiated cells (*20*–*22*). The stem-like cells persist long-term, maintain proliferative capacity, and give rise to terminally differentiated cells, whereas the terminally differentiated cells act as cytotoxic effector cells (*21*, *23*–*25*). PD-1/PD-L1 blockade acts on the stem-like cells and enhances their proliferation and differentiation into terminally differentiated cells (*20*, *21*, *23*, *26*). 4-1BB is highly expressed on Tim-3$^+$ terminally differentiated CD8 T cells compared to TCF1$^+$ stem-like cells in a tumor (*20*–*22*, *26*, *27*). However, the functional consequences of 4-1BB agonism on these cell populations are poorly understood.

In this study, we developed a tumor antigen–targeted mouse 4-1BB (m4-1BB) agonistic antibody, which consists of a tumor antigen–binding human IgG1 (hIgG1) and two m4-1BB agonistic single-chain variable fragments (scFvs). We targeted B7-H3 (CD276), a tumor antigen, which is overexpressed in a variety of human malignancies and tumor-associated vasculature (*28*, *29*), but not in healthy tissue. This bispecific antibody (bsAb; B7-H3×4-1BB) showed more potent T cell costimulatory activity in vitro and higher tumor localization compared to the 4-1BB agonistic mAb. B7-H3×4-1BB inhibited tumor growth in vivo without inducing 4-1BB agonistic mAb-associated irAE. Moreover, B7-H3×4-1BB acted on CD8 T cells, especially the Tim-3$^+$ terminally differentiated cells, to enhance their proliferation. B7-H3×4-1BB synergistically increased Tim-3$^+$ terminally differentiated cells with PD-1 blockade, followed by the eradication of established tumors. Last, we showed that the B7-H3×4-1BB platform is also applicable to h4-1BB.

RESULTS

Development of human B7-H3–targeted m4-1BB agonistic bsAb

We developed hIgG1 antibodies against B7-H3 and chose a clone, B5, as a candidate among several clones. The anti–B7-H3 mAb B5 bound specifically to human B7-H3 (hB7-H3), not to other proteins in the B7 family, as determined by enzyme-linked immunosorbent assay (ELISA) (fig. S1A). B5 binds to recombinant hB7-H3 with high affinity [dissociation constant (K_d) = 3.015 nM] assessed by surface plasmon resonance (SPR) analysis. B5 cross-reacted with monkey B7-H3 (cyB7-H3) with comparable binding potency and with mouse B7-H3 (mB7-H3) with lower affinity (fig. S1B). We also tested the binding capacity of B5 to the surface of human cancer cell lines (with or without hB7-H3 expression) and found that B5 recognized B7-H3–expressing human cell lines (fig. S1C). Using the scFvs derived from the anti–m4-1BB mAb 1D8 (*30*), we designed 1D8-scFv–linked anti–B7-H3 bsAb (B7-H3×4-1BB; clone: B5×1D8) with D265A/N297A (DANA) mutations (*31*) in the Fc region to inhibit Fcγ receptor (FcγR) binding (fig. S1D). B5×1D8 bound to both hB7-H3 and m4-1BB proteins determined by ELISA (fig. S1E). The heavy chain of B5×1D8 has a higher molecular weight (~75 kDa) compared to B5 and 1D8 (~50 kDa) because of the 1D8-scFv linked to the heavy chain, and the light chain of each antibody has a similar molecular weight (~25 kDa) (fig. S1F). Overall, the molecular weight of each antibody is as follows: B5×1D8 = ~200 kDa, B5 and 1D8 = ~150 kDa. B5×1D8 bound to activated mouse CD8 T cells by the interaction between 4-1BB and 1D8-scFv because the B5 did not bind to activate T cells (fig. S1G). We generated hB7-H3–overexpressing murine cancer cells by transfecting them with complementary DNA (cDNA) encoding hB7-H3 (MC38$^{hB7\text{-}H3}$, B16-F10$^{hB7\text{-}H3}$, and CT26$^{hB7\text{-}H3}$, respectively) and found that B5×1D8 bound to all three hB7-H3–overexpressing cells (fig. S1H). B5×1D8 showed marginal binding activities to the untransfected cells expressing mB7-H3 in variable levels. The tumor cells did not express 4-1BB; therefore, the weak binding activities of B5×1D8 in untransfected cells are possibly due to the cross-reactivity of B5 to mB7-H3 (fig. S1, I and J).

Functional characterization of B7-H3×4-1BB bsAb

To study the T cell costimulatory activity of B7-H3×4-1BB bsAb, we tested its effect on the up-regulation of CD25, CD44, and CD11c (*32*) on CD8 T cells and IFN-γ secretion in the presence of anti-CD3ε mAb and irradiated MC38$^{hB7\text{-}H3}$. Both B5×1D8 and 1D8 increased the expression of CD25, CD44, and CD11c, and IFN-γ secretion in a dose-dependent manner (Fig. 1, A and B), whereas hIgG1 isotype and B5 did not. In this experimental system, B5×1D8 was more potent compared to 1D8 and showed a lower half-maximal effective concentration (EC_{50}) (Fig. 1C). To determine B7-H3–dependent T cell costimulatory activity of B7-H3×4-1BB bsAb, we used untransfected MC38 cells as a control. B5×1D8 specifically induced the up-regulation of CD25 and CD44 on CD8 T cells in the presence of hB7-H3, but 1D8 up-regulated CD25 and CD44 regardless of hB7-H3 expression (Fig. 1D). We labeled 1D8, B5, and B5×1D8 with a near-infrared (NIR) fluorochrome to visualize each antibody. Mice bearing subcutaneously implanted MC38$^{hB7\text{-}H3}$ tumors were intravenously injected in the tail vein with NIR-labeled antibodies. The dose of each antibody was normalized on the basis of molarity. Tumor tissue and spleen were collected and imaged 24 hours after intravenous injection (Fig. 1E, left). B5×1D8 and B5 showed increased tumor localization with a tumor/spleen ratio of 3.50 ± 0.42 and 4.36 ± 0.63 (means ± SD), respectively, compared to that of 1D8 (1.60 ± 0.37), which corresponds to nonspecific tumor accumulation (Fig. 1E, right). The tumor/spleen ratio of B5×1D8 was slightly decreased compared to that of B5, although there was no statistical significance. As we used the same amount (based on molarity) of both antibodies, there might be a possibility that tumor vascular leakage may be hindered depending on the molecular weight of antibodies. In summary, B7-H3×4-1BB bsAb has a B7-H3–targeted CD8 T cell costimulatory activity and shows high tumor localization compared to the IgG-based 4-1BB agonistic antibody.

Absence of systemic irAEs following B7-H3×4-1BB bsAb treatment

We addressed the toxicity induced by 4-1BB stimulation by comparing B5×1D8 and 1D8. Naïve immunocompetent mice were intraperitoneally injected with hIgG1 isotype, B5×1D8, or 1D8 once a week for 4 weeks and euthanized a week later (fig. S2A). The treatment with B5×1D8 did not alter the BM cell population. In contrast, 1D8 decreased the total BM cells, accompanied by a decrease in CD19$^+$ B and NK cells, whereas T cells were increased (fig. S2B) as previously described (*13*). Liver toxicity is a major limitation of systemic administration of the 4-1BB agonist. Treatment with 1D8 significantly elevated the level of alanine aminotransferase (ALT) in the serum, which is a hallmark of liver damage (fig. S2C). There is no significant elevation of aspartate aminotransferase (AST) following 1D8 treatment. Apart from this, 1D8 induced enlargement of the liver as determined by weight, and increased infiltration of CD8 T cells, whereas infiltration of NK and CD4 T cells was decreased. However, B5×1D8 did not cause any change in the infiltration

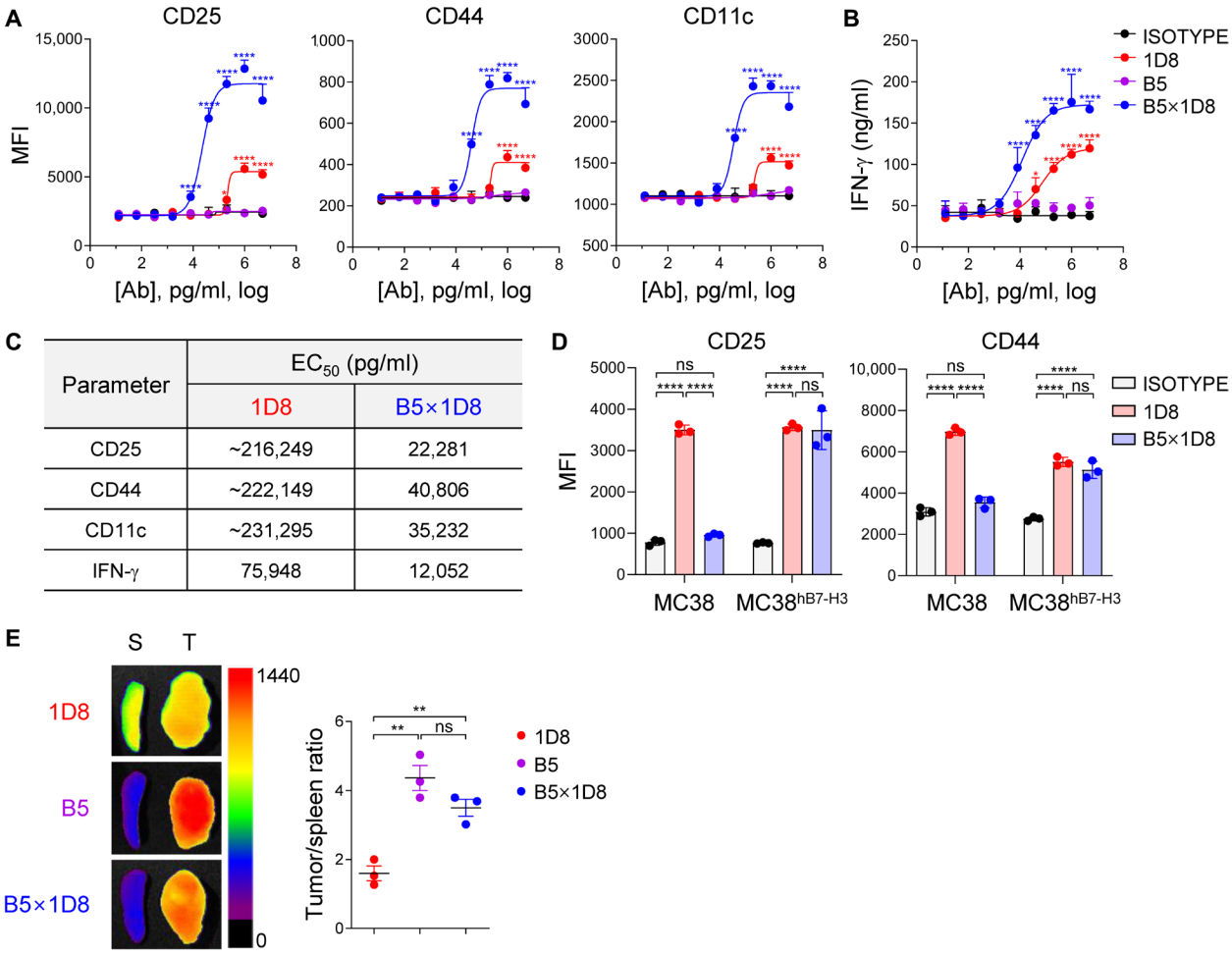

Parameter	EC_{50} (pg/ml)	
	1D8	B5×1D8
CD25	~216,249	22,281
CD44	~222,149	40,806
CD11c	~231,295	35,232
IFN-γ	75,948	12,052

Fig. 1. Functional characterization of B7-H3×4-1BB bsAb. (**A** and **B**) Dose-dependent costimulatory activity of hIgG1 isotype, 1D8, B5, and B5×1D8 on CD8 T cells stimulated with anti-CD3ε (1 μg/ml) and irradiated MC38$^{hB7\text{-}H3}$. Flow cytometric analysis of surface expression on CD8α$^+$ T cells (A) and IFN-γ secretion by ELISA (B) 72 hours after stimulation. (**C**) EC_{50} values for each parameter. (**D**) Flow cytometric analysis of surface expression on CD8α$^+$ T cells stimulated with anti-CD3ε (1 μg/ml) and irradiated wild-type MC38 or MC38$^{hB7\text{-}H3}$ with indicated antibodies (1 μg/ml) 72 hours after stimulation. (**E**) Representative ex vivo fluorescence images of spleen (S) and tumor (T) (left), and tumor/spleen ratio (right) from MC38$^{hB7\text{-}H3}$ tumor–bearing mice 24 hours after intravenous injection of 37.5 μg of 680XL-labeled mAb (1D8 and B5) or 50.0 μg of 680XL-labeled B5×1D8 ($n = 3$ per group). *$P < 0.05$; **$P < 0.01$; ***$P < 0.001$; and ****$P < 0.0001$, two-way analysis of variance (ANOVA) with Bonferroni posttests compared with hIgG1 isotype group (A and B), two-way ANOVA with Bonferroni posttests (D), and one-way ANOVA with Bonferroni's multiple comparison test (E). ns, not significant.

of immune cells into the liver (fig. S2D). 1D8 caused a reduction in the white blood cell counts at the time of analysis, accompanied by a decrease in the lymphocytes in the blood. 1D8 also increased the granulocyte population but did not affect the monocyte population in the blood, whereas B5×1D8 did not affect any of the complete blood counts (fig. S2E). Furthermore, treatment with 1D8 induced lymphadenopathy (fig. S2F) and splenomegaly (fig. S2G, left), as demonstrated by the weights of the corresponding tissues. The splenic immune cell composition was slightly altered following treatment with 1D8, including a decrease in NK cells and an increase in CD11b$^+$ cells, while treatment with B5×1D8 did not affect the immune cell composition in the spleen (fig. S2G, middle). Although 1D8 did not induce an increase in CD8 T cells in the spleen than the other tissues, the frequency of CD62L$^-$ CD44$^+$ effector CD8 T cells was elevated in the 1D8-treated mice (fig. S2G, right). Overall, the administration of B7-H3×4-1BB bsAb does not induce any of systemic irAEs, which were manifested by the IgG-based 4-1BB agonist treatment.

Antitumor activity of B7-H3×4-1BB bsAb

To study the antitumor efficacy of B7-H3×4-1BB bsAb, we used the MC38$^{hB7\text{-}H3}$ experimental tumor model (Fig. 2A). Injection of B5×1D8 in mice bearing MC38$^{hB7\text{-}H3}$ tumors (average diameter of 2 to 4 mm) resulted in eradicating tumors in 13 of 14 (93%) mice. Treatment with 1D8 resulted in complete regression in 13 of 14 (93%) mice, the same as that observed with B5×1D8 treatment (Fig. 2, B and C). These data indicate that the magnitude of the antitumor response provided by B7-H3×4-1BB bsAb was equivalent to that observed for the agonistic 4-1BB antibody 1D8. All mice treated with the hIgG1 isotype or B5 showed tumor progression and were euthanized within 6 weeks after the tumor cell injection (Fig. 2C). To test whether these treatments induced liver toxicity, we collected serum from each mouse 7 days after the final treatment. As in a previous result with naïve mice (fig. S2C), 1D8 treatment elevated serum ALT, whereas other treatments, including B5×1D8, did not (Fig. 2D).

To validate whether the tumor-targeted clustering of 4-1BB elicits the antitumor activity of B7-H3×4-1BB bsAb, we used the DANA-mutated

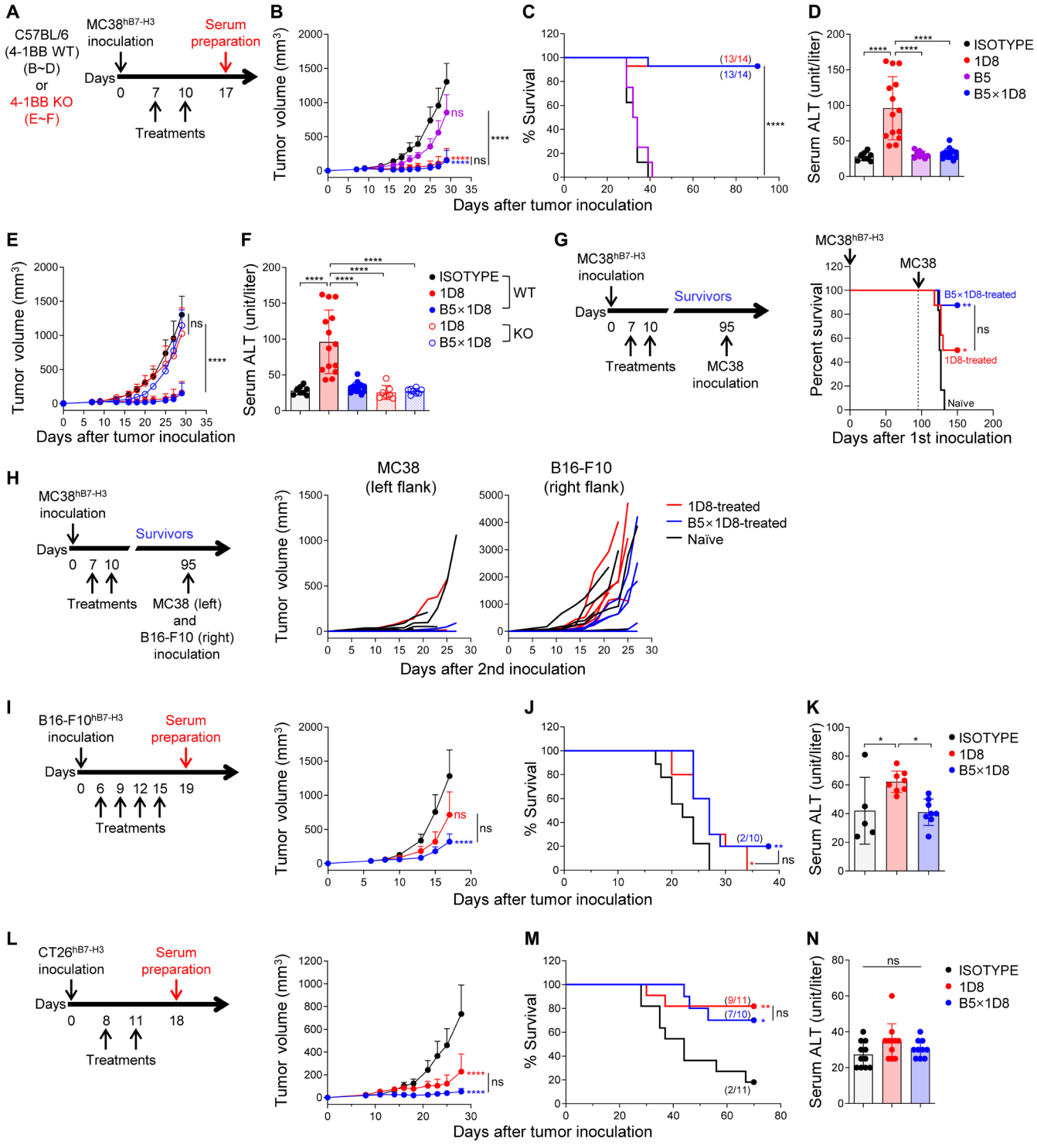

Fig. 2. Antitumor activity of B7-H3×4-1BB bsAb. (**A**) Experimental scheme of bsAb treatment in MC38$^{hB7\text{-}H3}$ tumor–bearing C57BL/6 or 4-1BB KO mice ($n = 7$ to 14 per group). WT, wild type. (**B** to **D**) Tumor growth curves (B), survival curves (C), and serum ALT (D) for each group of C57BL/6 mice. (**E** and **F**) Tumor growth curves (E) and serum ALT (F) for C57BL/6 or 4-1BB KO mice. (**G** and **H**) Experimental scheme for rechallenge of long-term survivors from 4-1BB agonist treatments (B) with MC38 alone (G) or both MC38 and B16-F10 (H). Survival curves for mice inoculated MC38 alone (G, right). Tumor growth curves for individual mice inoculated MC38 (H, middle) and B16-F10 (H, right). (**I** to **K**) B16-F10$^{hB7\text{-}H3}$ tumor–bearing C57BL/6 mice ($n = 10$ per group) treated with indicated antibodies. Tumor growth (I, right), survival (J), and serum ALT (K). (**L** to **N**) CT26$^{hB7\text{-}H3}$ tumor–bearing BALB/c mice ($n = 10$ to 11 per group) treated with indicated antibodies. Tumor growth (L, right), survival (M), and serum ALT (N). mAb (10.0 μg) and bsAb (13.3 μg) were used in all experiments. Numbers in survival curves indicate tumor-free mice/total mice at the end of the experiment. *$P < 0.05$; **$P < 0.01$; ***$P < 0.001$; and ****$P < 0.0001$, two-way ANOVA with Bonferroni posttests (B, E, I, and L), one-way ANOVA with Bonferroni's multiple comparison test (D, F, K, and N), and log-rank (Mantel-Cox) test (C, G, J, and M).

HER2×1D8 as a B7-H3 nonbinding control bsAb. HER2×1D8 failed to costimulate CD8 T cells in the presence of irradiated MC38$^{hB7\text{-}H3}$, while B5×1D8 costimulated T cells (fig. S3A). HER2×1D8 showed a marginal T cell costimulatory activity only in the presence of a cross-linking antibody, suggesting the clustering of bsAb is required for the costimulatory activity of anti–4-1BB scFv (fig. S3B). Consistently, treatment of HER2×1D8 could not induce the antitumor activity in MC38$^{hB7\text{-}H3}$ tumor–bearing mice (fig. S3C). These data demonstrated that the tumor antigen (B7-H3)–driven 4-1BB clustering is required for the antitumor activity of B5×1D8 and that the 4-1BB bivalency with 1D8-scFv alone cannot generate 4-1BB agonistic activity both in vitro and in vivo. To confirm that the host 4-1BB is required for the antitumor immune response induced by B5×1D8 or 1D8, we introduced MC38$^{hB7\text{-}H3}$ cells into 4-1BB knockout (KO) mice (Fig. 2A). Treatment with B5×1D8 or 1D8 did not induce tumor regression (Fig. 2E), with no elevation of serum ALT (Fig. 2F) in the 4-1BB KO mice. To investigate whether B7-H3×4-1BB bsAb could generate long-lasting and tumor-specific immunity, the mice that rejected the MC38$^{hB7\text{-}H3}$ tumor following treatment with B5×1D8 or 1D8 (Fig. 2C) were rechallenged with MC38 tumor cells alone or along with B16-F10 tumor cells (Fig. 2, G and H). Mice cured by B5×1D8 or 1D8 treatment were resistant to rechallenge with MC38 parental tumor cells but susceptible to irrelevant B16-F10 tumor cell challenge (Fig. 2, G and H), showing that the B7-H3–targeted 4-1BB costimulation could elicit long-lasting immunological memory specifically against MC38 tumors.

To study the antitumor activity of B7-H3×4-1BB bsAb in other murine tumor models, we used B16-F10$^{hB7\text{-}H3}$ and CT26$^{hB7\text{-}H3}$ tumor models. Treatment with B5×1D8 or 1D8 delayed tumor growth and increased the survival rate (Fig. 2, I and J) in the B16-F10$^{hB7\text{-}H3}$ tumor model. As in the MC38$^{hB7\text{-}H3}$ tumor model, 1D8 elevated the ALT level in the serum, whereas B5×1D8 did not (Fig. 2K). Injection of B5×1D8 and 1D8 in BALB/c mice bearing CT26$^{hB7\text{-}H3}$ tumors induced tumor regression in 7 of 10 (70%) and in 9 of 11 (81.8%) animals, respectively (Fig. 2, L and M). We did not observe significant differences in serum ALT following each treatment in the BALB/c mice (Fig. 2N). B16-F10 is known as a poorly immunogenic tumor, but MC38 and CT26 are regarded as immunogenic tumors with a higher mutational load (*33*, *34*). This different nature of tumor cells may lead to different outcomes after B7-H3×4-1BB bsAb treatment showing better responses against the immunogenic tumor model (MC38 and CT26) than the poorly immunogenic tumor model (B16-F10). Collectively, B7-H3×4-1BB bsAb generated a protective antitumor response without hepatotoxicity, and the antitumor activity was not tumor type and strain specific.

Role of CD8 T cells for B7-H3×4-1BB bsAb–mediated antitumor activity

The antitumor mechanism of IgG-based agonistic 4-1BB antibodies depends on the increase in antitumor CD8 T cells (*35*, *36*) and subsequent IFN-γ production (*34*). To determine whether B7-H3×4-1BB bsAb induces antitumor CD8 T cells, we analyzed the tumor-infiltrating lymphocytes (TILs) following the final treatment with bsAb (Fig. 3A). CD8 T cells were increased to 40% of the CD45$^+$ immune cells following B5×1D8 treatment, while CD8 T cells constituted less than 10% of the CD45$^+$ immune cells in the hIgG1 isotype–treated mice. Also, B5×1D8 treatment increased T_{reg} cells and decreased NK cells (Fig. 3A, left), although these changes were relatively marginal. We found that the expression of effector molecules (*37*) responsible for the suppressive functions of T_{reg}, such as CD25, CTLA-4, and granzyme B (GzmB) in intratumoral T_{reg} cells, was down-regulated following B5×1D8 treatment (fig. S4), suggesting a suppressive role of bsAb in T_{reg} function. The number of immune cells in the tumor showed a marked increase in CD8 T cells following B5×1D8 treatment (Fig. 3A, right), resulting in elevated CD8/T_{reg} ratio within the tumor microenvironment (TME) (Fig. 3B). B5×1D8 augmented the production of both IFN-γ and TNF-α in CD8 T cells (Fig. 3C), which is analogous to the reported action of 4-1BB agonistic mAbs. Consistently, we observed increased levels of IFN-γ and TNF-α in the tumor lysate following B5×1D8 treatment (Fig. 3D). B5×1D8 treatment increased the Ki-67–expressing CD8 T cells, which indicates cellular proliferation, leading to an increase in the number of proliferating CD8 T cells (Fig. 3E). However, we did not observe a significant difference in GzmB expression in CD8 T cells (Fig. 3F). Notably, 1D8 treatment displayed the functional activity similar to B5×1D8, augmenting the number and functions of CD8 T cells in tumors (fig. S5, A to C). Cell depletion experiments further confirmed the CD8-dependent activity of B5×1D8, showing that the antitumor efficacy of B5×1D8 was completely abrogated in the absence of CD8 T cells, while CD4 T and NK cells were dispensable (Fig. 3G), as shown in a previous report (*36*).

The analysis of immune cells in the tumor-draining lymph node (tdLN) showed no significant change of T cells after B5×1D8 treatment (fig. S5D). However, the frequencies of activated (CD44$^+$PD-1$^+$) and proliferating (Ki-67$^+$) CD8 T cells in the tdLN were up-regulated in the mice treated with 1D8, but not with B5×1D8 (fig. S5E). These data suggested that the increased number of CD8 T cells in tumors by B5×1D8 treatment is likely due to T cells' in situ proliferation within the tumor, but not the recruitment of proliferated T cells in the tdLN.

Increased PD-1$^+$ Tim-3$^+$ terminally differentiated CD8 T cells following B7-H3×4-1BB bsAb treatment

4-1BB is expressed on PD-1$^+$ CD8 T cells in the TME. Recent studies have shown that, among the PD-1$^+$ CD8 T cells, Tim-3$^+$ terminally differentiated cells highly express 4-1BB at the RNA level compared to TCF1$^+$ stem-like cells (*21*, *22*, *26*). Thus, we analyzed 4-1BB expression at the protein level in the CD8 T cell subpopulations in our MC38$^{hB7\text{-}H3}$ tumor model. We found 4-1BB expression only in the PD-1$^+$ CD8 T cells, especially in the Tim-3$^+$ terminally differentiated cells, 7 days after the tumor injection (fig. S6). Similar to RNA expression of 4-1BB in previous reports, TCF1$^+$ stem-like cells do not express the 4-1BB protein (fig. S6B).

To study the impact of 4-1BB agonists on each CD8 T cell subpopulation, we treated MC38$^{hB7\text{-}H3}$ tumor–bearing mice with B5×1D8. As in the previous experiment, we analyzed the TIL population 4 days after the final treatment. B5×1D8 treatment significantly increased the number of PD-1$^+$Tim-3$^+$ terminally differentiated CD8 T cells (Fig. 4A). We further dissected the change within the CD8 T cell subpopulations with TCF1 and found that treatment with the 4-1BB agonist decreased the frequency of TCF1$^+$Tim-3$^-$ cells within the PD-1$^+$ CD8 T cells but did not significantly alter TCF1$^-$Tim-3$^+$ PD-1$^+$ CD8 T cells (Fig. 4B). Given the expression of 4-1BB in Tim-3$^+$ terminally differentiated cells, our results suggest that 4-1BB agonists act on terminally differentiated cells and enhance their amplification in the tumor. The expression pattern of transcription factors such as Eomesodermin (Eomes) and T-box expressed in T cells (T-bet) is also linked to the differentiation of CD8 T cells in the

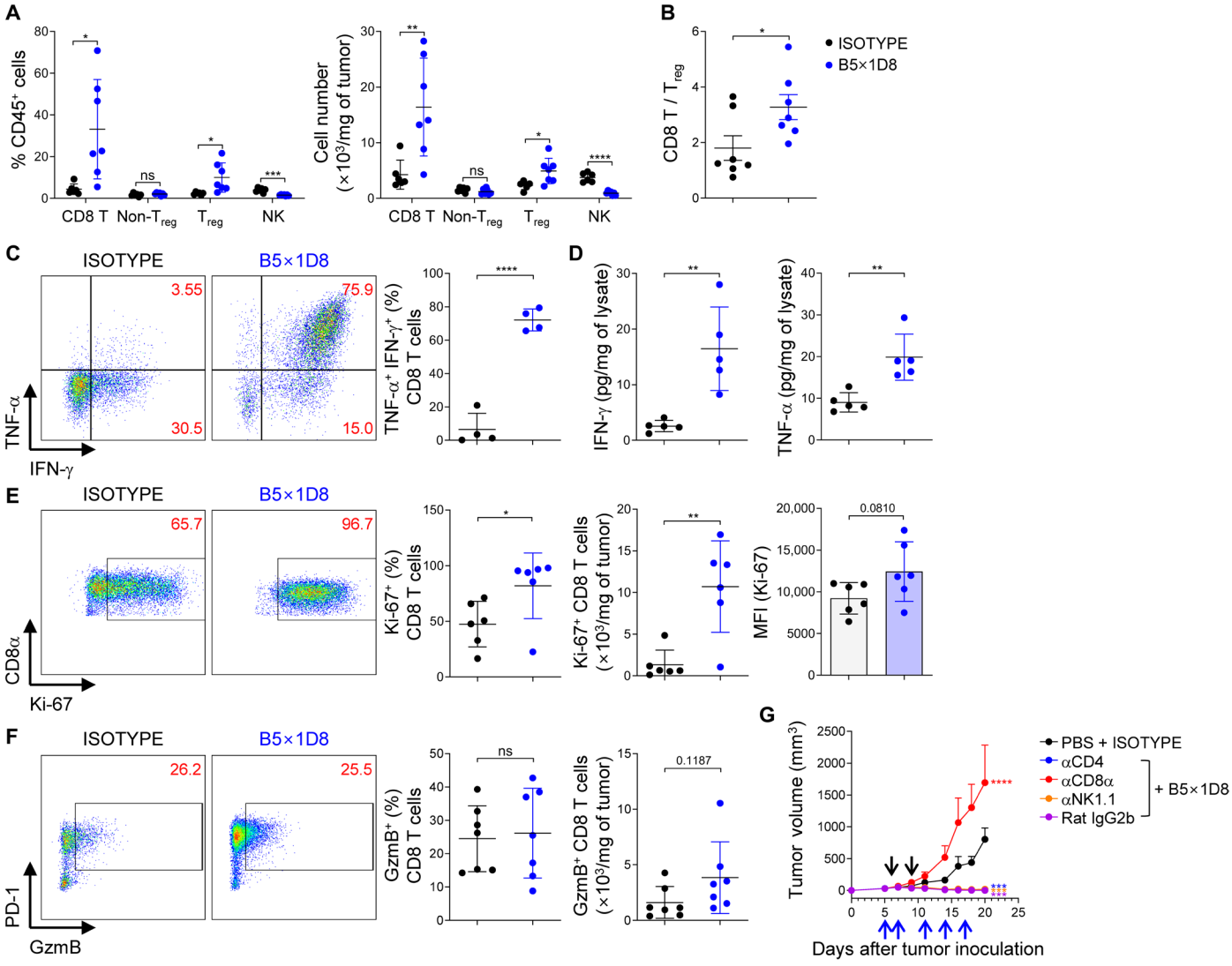

Fig. 3. Role of CD8 T cells for B7-H3×4-1BB bsAb–mediated antitumor activity. MC38$^{hB7\text{-}H3}$ tumor–bearing C57BL/6 mice ($n = 4$ to 7 per group) were treated, as shown in Fig. 2A. Tumor tissues were analyzed 4 days after the last treatment. (**A**) Flow cytometric analysis of TIL composition (left) and cell count per milligram of the tumor (right). (**B**) CD8 T cell/T_{reg} cell ratio. (**C**) TNF-α and IFN-γ in restimulated CD8 TILs. (**D**) Levels of TNF-α and IFN-γ in the tumor lysate by ELISA. (**E** and **F**) Flow cytometric analysis of Ki-67 (E) and GzmB (F) expression in CD8 TILs. The numbers in each plot indicate the percentage of cells expressing each molecule. Representatives of two independent experiments were shown. (**G**) Tumor growth from MC38$^{hB7\text{-}H3}$ tumor–bearing C57BL/6 mice ($n = 7$ per group) treated with 10.0 μg of hIgG1 isotype or 13.3 μg of B5×1D8 and 200 μg of depletion antibody. Black and blue arrows indicate treatment points and depletion antibody injection points, respectively. *$P < 0.05$; **$P < 0.01$; ***$P < 0.001$; and ****$P < 0.0001$, unpaired Student's t test (A to F) and two-way ANOVA with Bonferroni posttests compared with phosphate-buffered saline (PBS) + ISOTYPE–treated group (G).

TME. The terminally differentiated CD8 T cells express a high level of Eomes but a low T-bet (*38*, *39*). A previous report showed that the 4-1BB agonist increases the level of Eomes and does not change in the level of T-bet in KLRG1$^+$ CD8 T cells from mice bearing B16 tumor (*40*). Similarly, we found an increase in Eomes, but no change in T-bet expression, within the PD-1$^+$ CD8 T cells following B5×1D8 treatment (Fig. 4C). Therefore, these results also suggest that B7-H3×4-1BB bsAb increases terminally differentiated CD8 T cells in the tumor.

Synergistic effect of B7-H3×4-1BB bsAb with PD-1 blockade

4-1BB agonist treatment synergized with ICBs, such as anti–PD-1 in various mouse tumors (*41*–*43*). To test the antitumor effect of B7-H3×4-1BB bsAb in combination with anti–PD-1 in an advanced tumor model, we started treating MC38$^{hB7\text{-}H3}$ tumor–bearing mice 12 to 14 days after the tumor injection (when the tumor reached an average volume of 100 to 200 mm^3; Fig. 5A). Treatment with anti–PD-1 or B5×1D8 alone showed significant inhibition of tumor growth compared to the isotype control–treated group (Fig. 5B). Treatment with B5×1D8 alone resulted in complete tumor regression in 2 of 10 (20%) mice (Fig. 5, C and D). B5×1D8 and anti–PD-1 combination therapy synergistically inhibited tumor growth (Fig. 5B) and induced complete tumor regression in 7 of 10 (70%) mice (Fig. 5, C and D). These data indicate that B7-H3×4-1BB bsAb generates a synergistic antitumor response with PD-1 blockade. We also tried combination therapy with other ICBs such as anti–CTLA-4

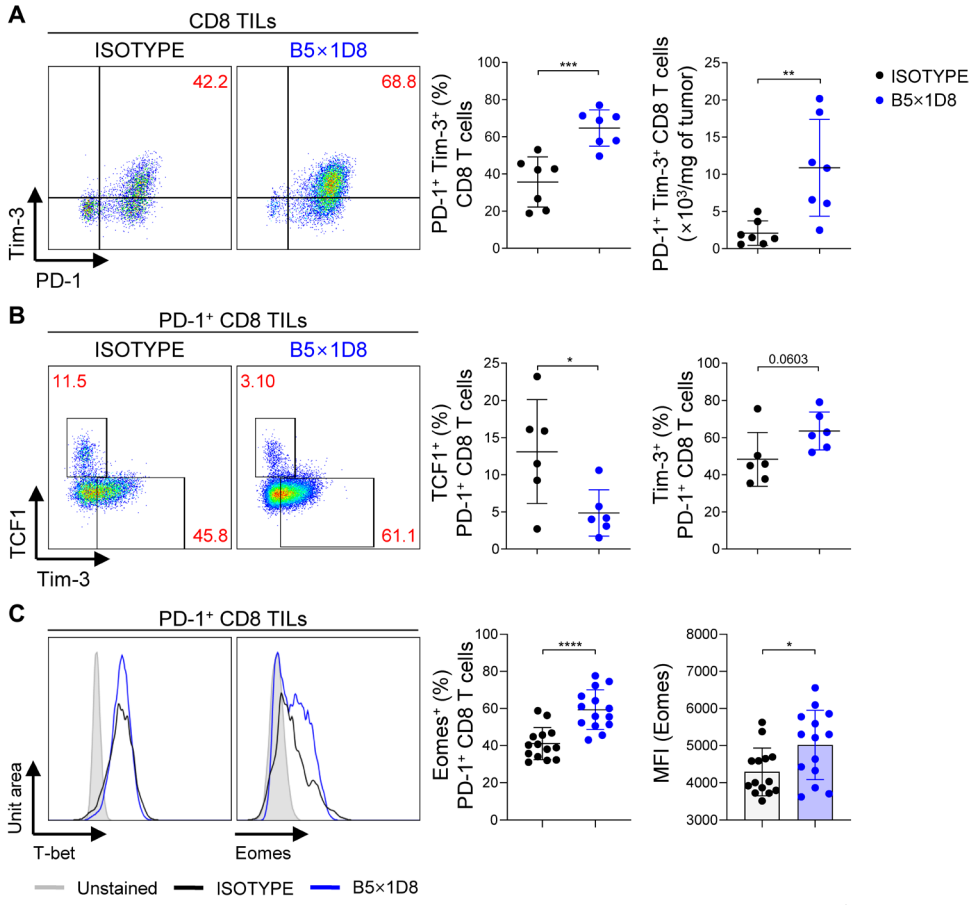

Fig. 4. Increased PD-1$^+$Tim-3$^+$ terminally differentiated CD8 T cells following B7-H3×4-1BB bsAb treatment. (**A** to **C**) MC38$^{hB7\text{-}H3}$ tumor–bearing C57BL/6 mice ($n = 6$ to 14 per group) were treated as in Fig. 3, and TILs were analyzed by flow cytometry 4 days after the last treatment. (A) Surface expression of PD-1 and Tim-3 on CD8 TILs. Expression of Tim-3 and TCF1 (B), and T-bet and Eomes (C) in CD8 TILs. Mean fluorescence intensity (MFI) of Eomes in PD-1$^+$ CD8 TILs was represented (C, right). The numbers in each plot indicate the percentage of cells expressing each molecule. Dots on the right are representative of three independent experiments. *$P < 0.05$; **$P < 0.01$; ***$P < 0.001$; and ****$P < 0.0001$, unpaired Student's t test.

and anti–Tim-3, because 4-1BB agonistic antibodies showed synergy with those ICBs in mounting antitumor activity in previous studies (*44*, *45*). However, the blockade of CTLA-4 or Tim-3 did not augment the antitumor activity of B5×1D8 (fig. S7).

In contrast to the palpable tumor model, B5×1D8 treatment alone did not increase CD8 T cells in the advanced tumors; however, the combination of B5×1D8 and anti–PD-1 markedly increased CD8 T cells (Fig. 5E). The frequency of proliferating (Ki-67$^+$) CD8 T cells was not changed (Fig. 5F), but GzmB-expressing CD8 T cells were increased in the anti–PD-1–treated or combination-treated mice (Fig. 5G). B5×1D8 or anti–PD-1 alone increased Tim-3$^+$ terminally differentiated cells in the advanced tumors, with the TCF1$^+$ stem-like CD8 T cells remaining unchanged (Fig. 5H). However, the combination of B5×1D8 with anti–PD-1 further up-regulated the proportion of terminally differentiated CD8 T cells, whereas the stem-like cells were down-regulated (Fig. 5H), resulting in increased terminally differentiated to stem-like cell ratio. These data suggest that the strong antitumor activity elicited by the combination regimen correlates with an increase in terminally differentiated CD8 T cells in the TME. Recently, Miller *et al.* showed that anti–PD-1 acts preferentially on TCF1$^+$ stem-like CD8 T cells, resulting in the proliferation and differentiation of these cells into Tim-3$^+$ terminally differentiated cells (*20*, *21*). Therefore, these data suggest that PD-1 blockade and B7-H3×4-1BB bsAb target different subsets of CD8 T cells in the TME, such as the stem-like and terminally differentiated cells, respectively, ultimately increasing the population of fully differentiated effector CD8 T cells that exerts tumoricidal function.

Functionality and antitumor efficacy of B7-H3×4-1BB bsAb in PBMC and h4-1BB KI mice

On the basis of the previous studies in mice, we next sought to determine the effect of B7-H3×4-1BB bsAb on the h4-1BB system. To do this, we first generated an anti–h4-1BB mAb, 1A10. The binding epitope of 1A10 was different from that of the urelumab analog, a reference ligand nonblocking anti–h4-1BB agonistic mAb (*46*). 1A10 clone also does not block human 4-1BBL binding to h4-1BB, like ligand nonblocking 1D8 clone (*30*) used in the mouse study. The urelumab analog activates 4-1BB signaling without engagement; however, 1A10 activates 4-1BB signaling only after engaging with the cross-linking antibodies (fig. S8). Next, we generated a 1A10-scFv–linked anti–B7-H3 bsAb, B5×1A10, and compared the pharmacokinetics of B5 and B5×1A10 in mice. These two antibodies have similar pharmacokinetic profiles; serum half-life ($T_{1/2}$) of B5 was 6.7 ± 0.4 days, and $T_{1/2}$ of B5×1A10 was 6.3 ± 0.3 days in naïve

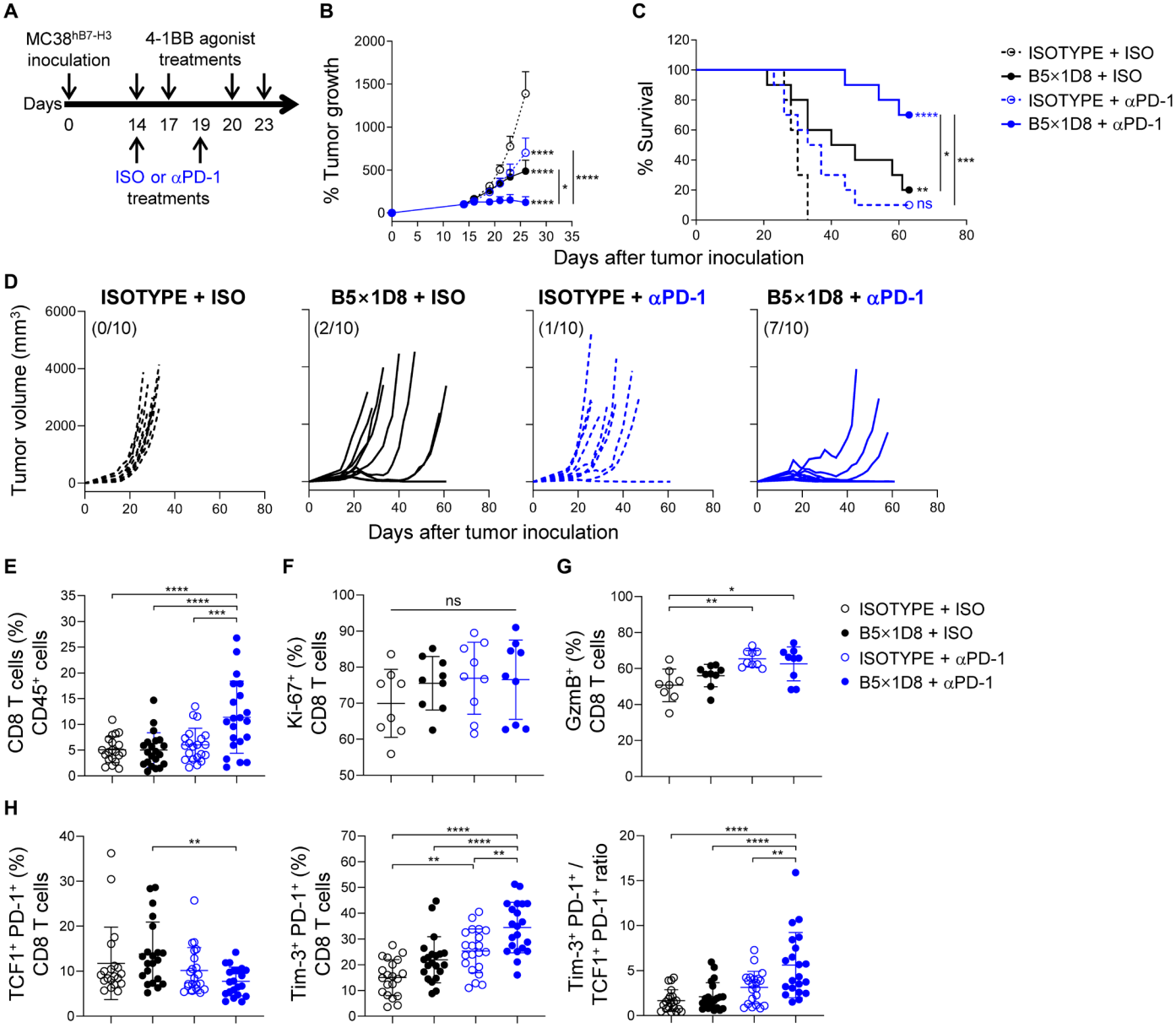

Fig. 5. Synergistic effect of B7-H3×4-1BB bsAb with PD-1 blockade on tumor growth and development of terminally differentiated CD8 T cells. (**A**) Experimental scheme of combination therapy of bsAb and anti–PD-1 in MC38$^{hB7\text{-}H3}$ tumor–bearing C57BL/6 mice ($n = 10$ per group). mAb (37.5 μg) and bsAb (50.0 μg) were treated with rat IgG2a isotype (ISO) or anti–PD-1 (200 μg). (**B** to **D**) Tumor growth curves (B), survival curves (C), and tumor growth curves for individual mice (D). Numbers in each plot in (D) indicate tumor-free/total mice ratios. (**E** to **H**) Flow cytometric analysis of CD8 T cells (E), Ki-67 (F), and GzmB (G) expression on CD8 T cells, TCF1$^+$PD-1$^+$ stem-like CD8 T cells (H, left), Tim-3$^+$PD-1$^+$ CD8 T cells (H, middle), and Tim-3$^+$PD-1$^+$ CD8 T cell/TCF1$^+$PD-1$^+$ CD8 T cell ratio (H, right) at day 20. Data represent means ± SD of pooled biologically independent samples from three independent experiments ($n = 6$ to 9 per group) for (E) and (H). *$P < 0.05$; **$P < 0.01$; ***$P < 0.001$; and ****$P < 0.0001$, two-way ANOVA with Bonferroni posttests (B), log-rank (Mantel-Cox) test (C), and one-way ANOVA with Bonferroni's multiple comparison test (E to H).

mice after single intravenous injection. These data indicate that bsAb behaves similarly to a conventional mAb in mice.

To test the 4-1BB agonistic activity of B5×1A10, we cocultured h4-1BB–expressing reporter cells with B7-H3–expressing cells, including MCF-7, HCC1954, MDA-MB-231, and PANC-1 cells, and found that B5×1A10 activated the nuclear factor κB (NFκB) signaling pathway downstream of the 4-1BB receptor. In contrast, B5×1A10 did not activate the NFκB pathway with KATO III cells (Fig. 6A), which do not express B7-H3 (fig. S1C). The urelumab analog activates 4-1BB signaling regardless of B7-H3 expression on the cells (Fig. 6A). Thus, these data indicate that B5×1A10 needs tumor antigen–mediated 4-1BB receptor clustering for their activity. Furthermore, we used human peripheral blood mononuclear cells (PBMCs) to test whether B5×1A10 could activate primary human CD8 T cells. PBMCs were cocultured with B7-H3^{high} HCC1954 cells with different concentrations of 4-1BB agonists, including 1A10, B5×1A10, and the urelumab analog. B5×1A10 increased IFN-γ secretion (Fig. 6B) and tumor cell lysis (Fig. 6C) with much higher efficacy

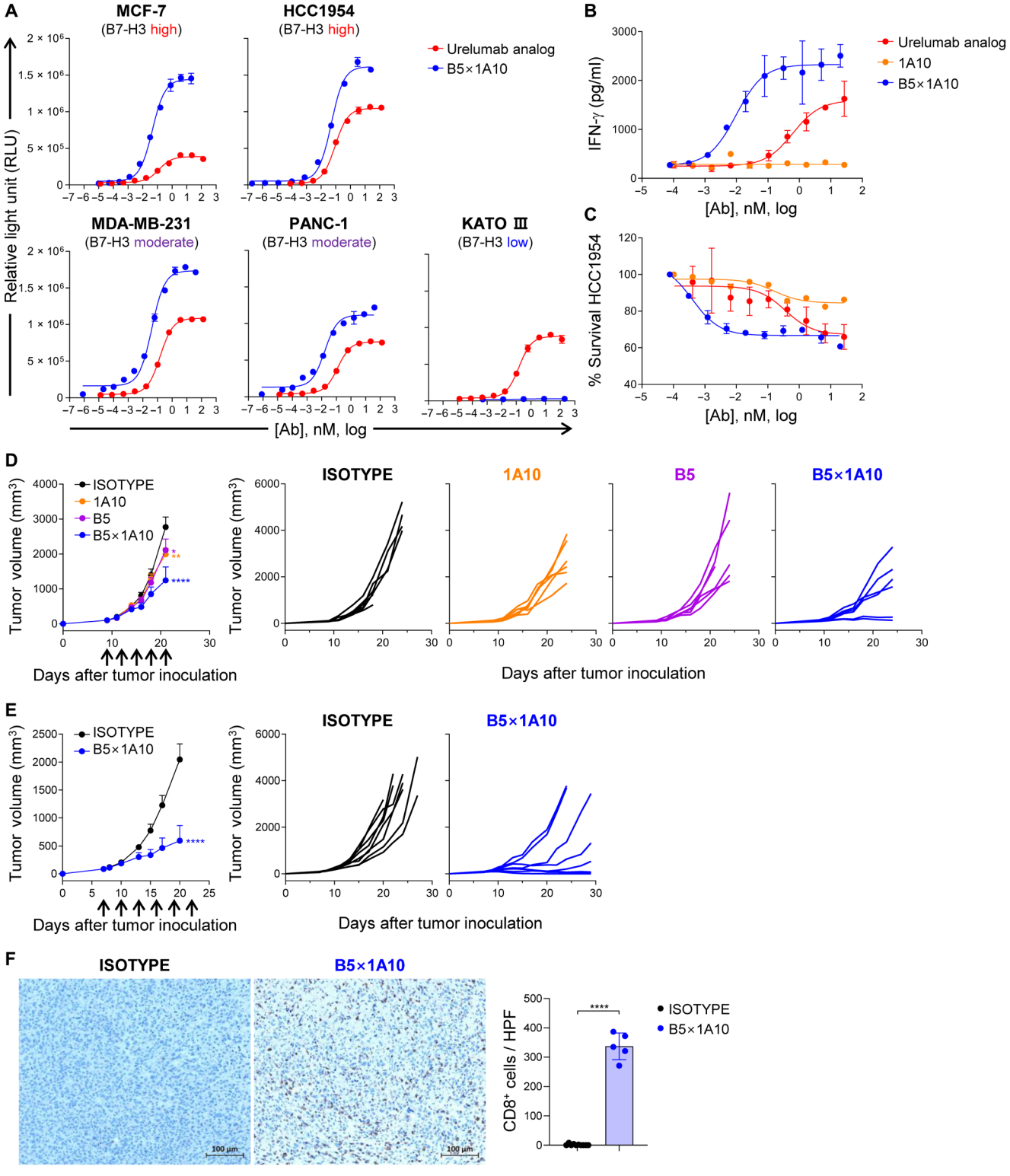

Fig. 6. Antitumor efficacy of B7-H3×4-1BB bsAb in the human system. (**A**) Dose-dependent costimulatory activity of the urelumab analog and B5×1A10 on Jurkat-NFκB-luc2/h4-1BB reporter cells. Luminescence was measured 6 hours after stimulation. (**B** and **C**) Dose-dependent costimulatory activity of the urelumab analog, 1A10, and B5×1A10 on PBMCs stimulated with anti-human CD3 (5 μg/ml) and HCC1954 cells. IFN-γ secretion by ELISA (B) and optical cellular density by cell counting kit (C) 72 hours after stimulation. (**D** and **E**) MC38$^{hB7\text{-}H3}$ tumor–bearing h4-1BB KI mice ($n = 6$ to 8 per group) were treated with indicated antibodies. Black arrows indicate treatment points. Tumor growth curves of individual mice are shown on the right. (**F**) Representative immunohistochemistry images (left) showing CD8 expression (brown) in tumor tissue from mice in (D). Infiltrating CD8$^+$ cell counts in a high-power field (HPF; 20×) at randomly selected tumor areas (right). Nuclear staining with hematoxylin is in blue. Scale bars, 100 μm. *$P < 0.05$; **$P < 0.01$; ***$P < 0.001$; and ****$P < 0.0001$, two-way ANOVA with Bonferroni posttests (D and E) and unpaired Student's t test (F).

than the urelumab analog. In contrast, 1A10 alone could not activate human PBMCs.

Last, we evaluated the in vivo antitumor efficacy of B5×1A10 on MC38$^{hB7\text{-}H3}$ tumors in the h4-1BB knock-in (KI) mice. Treatment of h4-1BB KI mice bearing established MC38$^{hB7\text{-}H3}$ tumors with B5 and hIgG1 isotype failed to suppress tumor growth (Fig. 6D). In contrast, administration of B5×1A10 inhibited tumor growth in the h4-1BB KI mice, although its antitumor effects were slightly variable between two independent experiments (Fig. 6, D and E). Consistent with the previous data (Fig. 3A), CD8$^+$ cells significantly increased in tumor tissue following B5×1A10 treatment (Fig. 6F). Collectively, these data suggest that B5×1A10 can be used as immunotherapy for patients with B7-H3–positive cancer.

DISCUSSION

Agonistic anti–h4-1BB antibodies have not advanced beyond early clinical trials because of severe hepatotoxicity (urelumab) and low efficacy (utomilumab) (*7*). To overcome these issues, several groups have attempted using bispecific approaches to restrict 4-1BB agonism in a tumor-specific manner by simultaneously targeting TAA: EGFR-targeted trimerbody (*17*), FAP or CD19-targeted 4-1BBL (*18*), and HER2-targeted 4-1BB agonistic anticalin (*19*). Treatment with these 4-1BB bispecifics has provided proof of concept by showing antitumor efficacy with significantly reduced irAEs. However, several issues need to be resolved to further improve the 4-1BB bispecifics, for example, adopting more tumor-specific antigens, applying in combination with other cancer therapy like ICBs, and understanding the mode of action through which 4-1BB bispecifics regulate T cells in the TME. Here, we present an alternative bsAb, the B7-H3–targeted 4-1BB agonistic bsAb (B7-H3×4-1BB), which is a tetravalent IgG-scFv bispecific form containing DANA mutation in the IgG backbone to eliminate FcγR binding. B7-H3×4-1BB bsAb binds to B7-H3 and 4-1BB simultaneously, which leads to 4-1BB clustering through the cross-linking of B7-H3–binding arms in the TME. In healthy tissues, neither B7-H3 binding nor FcγR binding–mediated 4-1BB clustering occurs, resulting in the absence of toxicity (fig. S9A).

Immunotherapies targeting B7-H3, including chimeric antigen receptor T cells, are currently under clinical investigation in multiple solid tumors (NCT02982941, NCT01391143, and NCT04185038), highlighting B7-H3 as an effective therapeutic target for cancer. The expression of B7-H3 in a steady state at the protein level is quite limited in healthy tissues, although mRNA expression of B7-H3 has been reported in multiple organs. Numerous reports have described the overexpression of B7-H3 protein in various types of cancer, including colorectal cancer, melanoma, and atypical teratoid/rhabdoid tumors (*47*). Tumor cells and tumor-associated endothelial and stromal cells also express B7-H3 at the cell surface (*28*, *29*, *48*). High expression of B7-H3 within the tumor tissue is correlated with bad prognosis, poor clinical outcome, and lymph node metastasis (*49*). The molecular mechanism of B7-H3–mediated tumor growth and immune evasion remains unclear. B7-H3 is believed to be a coinhibitory receptor in the B7-CD28 pathway (*50*, *51*), and the interaction with an as-yet-unidentified ligand decreases the proliferation and cytokine production of T cells (*52*). Given the immunoregulatory role of B7-H3, the blockade of B7-H3 induces antitumor activity (*29*, *53*). The anti–B7-H3 antibody (B5) used in this study also reversed B7-H3–mediated T cell inhibition in vitro. Therefore, B7-H3×4-1BB bsAbs could provide B7-H3 blocking effects along with 4-1BB agonism on the T cells within the tumor tissue. Because of the low cross-reactivity of B5 mAb with mB7-H3, we did not observe any antitumor activity in murine tumor models in this study following treatment with B5 mAb alone. However, it is tempting to speculate that the anti–B7-H3 arm of the 4-1BB bispecifics may play dual roles in humans: tumor-specific targeting and suppression of immune regulation through B7-H3.

The antitumor effect of B7-H3×4-1BB bsAb is mainly mediated by CD8 T cell immunity to tumors, as observed in 4-1BB agonistic mAbs. We also observed a marginal increase in T_{reg} cells and, interestingly, down-regulation of effector molecules (CD25, CTLA-4, and GzmB) in T_{reg} cells following B7-H3×4-1BB bsAb treatment. These data suggest that B7-H3×4-1BB bsAb may decrease suppressive functions of T_{reg} cells and elicit antitumor immunity by cooperatively modulating CD8 T cells and T_{reg} cells, although further investigation is needed on the role of intratumoral T_{reg} cells in the B7-H3×4-1BB–mediated antitumor immunity. Also, we found that B7-H3×4-1BB bsAb acts on the tumor-infiltrating CD8 cells, only a fraction of which express 4-1BB, suggesting that the regulation of 4-1BB$^+$ CD8 TILs by bsAb in tumors is the prime mode of its antitumor action. Recent studies have reported two functionally distinct CD8 TIL subsets, the TCF1$^+$ stem-like and Tim-3$^+$ terminally differentiated populations, which distinctly express the immune checkpoint molecules (*20*–*22*). Effective tumor control requires both cell populations; terminally differentiated cells act as short-lived primary cytotoxic effector cells, whereas the stem-like cells are poorly cytotoxic but act as a reservoir to replenish the terminally differentiated cell population (*21*, *23*–*25*). B7-H3×4-1BB bsAb appears to target the Tim-3$^+$ terminally differentiated CD8 TILs that express 4-1BB protein at a high level for augmenting their proliferation and functions, and collectively increases the number of tumoricidal CD8 TILs. In contrast, the TCF1$^+$ stem-like CD8 TILs do not respond to bsAb, likely because of the absence of 4-1BB expression. Although both stem-like and terminally differentiated CD8 T cells express PD-1, the blockade of PD-1/PD-L1 interaction affects the stem-like cells, enhancing their proliferation and differentiation into terminally differentiated cells (*20*, *21*, *23*, *26*) that are the main targets of B7-H3×4-1BB bsAb. Therefore, combination therapy with anti–PD-1 and bsAb targets distinct cell populations to synergistically increase Tim-3$^+$ terminally differentiated CD8 TILs, leading to improved antitumor activity (fig. S9B).

In summary, our study presents a bispecific 4-1BB agonistic antibody based on the IgG-scFv. This bsAb has potent antitumor efficacy against multiple tumors and does not induce 4-1BB–mediated toxicity. The in situ activation of 4-1BB by bsAb in tumors specifies its target to the tumoricidal effector CD8 T cells and cooperates with PD-1 blockade, which replenishes the precursors of the effector CD8 T cells. Recent data collected from human cancer patients suggest that 4-1BB is predominantly expressed on PD-1^{hi}Tim-3$^+$ terminally differentiated CD8 TILs (*54*, *55*). These 4-1BB–expressing CD8 T cells showed higher proliferative potential and were further enhanced by PD-1 blockade (*56*). Therefore, B7-H3×4-1BB bsAb represents a promising immunotherapeutic against human cancers.

MATERIALS AND METHODS

Expression and purification of recombinant antibodies

For expression of recombinant antibodies, synthetic genes encoding the mAb (B5, 1D8, urelumab analog, and 1A10) or bsAb (HER2×1D8,

B5×1D8, and B5×1A10) were subcloned into pcDNA 3.4-TOPO plasmid using the pcDNA 3.4-TOPO TA Cloning Kit (Thermo Fisher Scientific, A14308). To produce recombinant antibodies, plasmids encoding each antibody were transfected to ExpiCHO-S cells (Thermo Fisher Scientific, A29127) using the ExpiCHO Expression System Kit (Thermo Fisher Scientific, A29133, containing ExpiFectamine CHO Reagent, ExpiFectamine CHO Enhancer, and ExpiCHO Feed). ExpiCHO-S cells were maintained in a shaking incubator at 37°C with 8% CO_2 and prepared by diluting the ExpiCHO Expression Medium (Thermo Fisher Scientific, A29100) at a cell concentration of 6×10^6 cells/ml on the day of transfection. The ExpiFectamine CHO Reagent/plasmid complex was prepared in OptiPRO SFM (Thermo Fisher Scientific, 12309), incubated for 5 min at room temperature, and then transferred to the prepared cells. After 20 hours of incubation, ExpiFectamine CHO Enhancer (used to enhance protein production) and ExpiCHO Feed (used to support long-term, high-density transient transfection) were added and then further incubated for 7 to 10 days. Recombinant antibodies were purified from the cell culture fluid by protein A affinity chromatography using a HiTrap MabSelect SuRe column (GE Healthcare, 28-4082-55). The column was equilibrated by equilibration buffer [50 mM tris-HCl (pH 7.4), 100 mM NaCl] and then loaded with cell culture fluid. The antibody was eluted using elution buffer (50 mM citrate, pH 3.4) and then neutralized to pH 6.5 using 1 M tris-HCl (pH 9.0). Purified antibodies were concentrated in formulation buffer (20 mM histidine, 7% trehalose) by ultrafiltration using an Amicon Ultra 15 30K device (Merck, UFC903096), and protein concentrations were measured using NanoDrop One (Thermo Fisher Scientific). Endotoxin levels were ≤1.0 endotoxin unit (EU)/mg as measured by Endosafe nexgen-PTS (Charles River Laboratories).

Cell lines and culture conditions

Mouse cancer cells, MC38, a C57BL/6 colon adenocarcinoma cell line, were purchased from Kerafast (ENH204-FP), and B16-F10, a C57BL/6 skin melanoma cell line, and CT26, a BALB/c colon carcinoma cell line, were purchased from the American Type Culture Collection (ATCC) (CRL-6475 and CRL-2638, respectively). MC38 cells were grown in Dulbecco's modified Eagle's medium (DMEM; Welgene, LM001-05) supplemented with 10% fetal bovine serum (FBS; GE Healthcare Life Sciences, SH30084.03), 1× anti-anti (Gibco, 15240), 1× GlutaMAX (Gibco, 35050), 10 mM Hepes (Gibco, 15630), 1 mM sodium pyruvate (Gibco, 11360), 0.1 mM MEM nonessential amino acids (Gibco, 11140), and gentamicin (50 μg/ml; Gibco, 15750). B16-F10 cells were grown in DMEM supplemented with 10% FBS and 1× anti-anti. CT26 cells were grown in RPMI 1640 (Welgene, LM011-01) supplemented with 10% FBS and 1× anti-anti. To establish hB7-H3–overexpressing murine tumor cell lines, each cell line was transfected with B7-H3 (CD276) (NM_001024736) Human Tagged ORF Clone (OriGene, RC215064) using Lipofectamine 3000 transfection reagent (Thermo Fisher Scientific, L3000). Stably transfected clones were selected at a concentration of G-418 (700 μg/ml; AG Scientific, G-1033) for $MC38^{hB7\text{-}H3}$ cells and 500 μg/ml for $B16\text{-}F10^{hB7\text{-}H3}$ and $CT26^{hB7\text{-}H3}$ cells. Human cancer cells, MCF-7 (HTB-22), PANC-1 (CRL-1469), KATO III (HTB-103), and HCC1954 (CRL-2338), were purchased from ATCC. MDA-MB-231 was purchased from the Korean Cell Line Bank (30026). MCF-7 and PANC-1 cells were grown in DMEM/F12 (Gibco, 11330) supplemented with 10% FBS (Gibco, 10099) and 1× anti-anti. HCC1954 and MDA-MB-231 cells were grown in RPMI 1640 (Gibco, 22400) and 1× anti-anti. KATO III cells were grown in Iscove's modified Dulbecco's medium (IMDM) (Gibco, 12440). All cells were grown at 37°C in a humidified incubator with 5% CO_2.

Mice

We use 6-week-old female C57BL/6 (Orient Bio Inc.), 6- to 8-week-old female in-house bred BALB/c, and 6- to 12-week-old 4-1BB KO mice (C57BL/6 background; a gift from B. Kwon, University of Ulsan, Korea). All mouse strains were maintained under specific pathogen–free (SPF) conditions in an approved animal facility at POSTECH Biotech Center. All animal experiments were conducted according to the protocols approved by the Institutional Animal Care and Use Committee of POSTECH.

h4-1BB KI mice [B-hCD137 (4-1BB) mice, C57BL/6-*Tnfrsf9*$^{tm1(TNFRSF9)/Bcgen}$/Bcgen, stock number: 110004], whose 4-1BB gene is replaced by the h4-1BB gene, were supplied by Jiangsu Biocytogen Co. Ltd. These mice were housed in an SPF barrier at the animal center of Beijing Biocytogen Co. Ltd. Eight-week-old female h4-1BB KI mice were acclimated for 3 days to 1 week after arrival and used for experiments in Biocytogen Haimen Animal Center.

Mouse T cell costimulation assay

Tumor cells were irradiated (5 Gy) with an X-RAD 320 irradiator (Precision X-Ray Inc.), and 1×10^4 tumor cells were seeded in a 96-well plate. Spleens from C57BL/6 mice were dissociated into a single-cell suspension using a 40-μm cell strainer, treated with red blood cell lysis buffer (Sigma-Aldrich, R7757), and further passed through a 100-μm cell strainer. A splenic single-cell suspension was then resuspended in complete IMDM (cIMDM) (Welgene, LM004-01) supplemented with 10% FBS, 1× anti-anti, and 55 μM 2-mercaptoethanol (Gibco, 21985). Splenocytes (5×10^5) were placed in a 96-well plate and cultured with In Vivo Ready anti-mouse CD3ε mAb (1 μg/ml) (clone: 145-2C11; Tonbo Biosciences, 40-0031) alone or with purified antibodies at the indicated dose. For cross-linking HER2×1D8, hIgG1 κ (1 μg/ml) (Southern Biotech, 0151K-01) was added. Seventy-two hours after culture, T cell activation was analyzed by flow cytometry, and supernatants were collected and assayed for IFN-γ secretion by ELISA using a mouse IFN-γ DuoSet ELISA kit (R&D Systems, DY485).

Antibody binding assay

For the study on binding characteristics of anti–B7-H3 mAb or B7-H3×4-1BB bsAb by ELISA, 0.1 μg of the following B7 family antigens [diluted in phosphate-buffered saline (PBS)] was coated on Nunc Maxisorp plates overnight at 4°C: hB7-H3/CD276/His tag (11188-H08H), human B7-1/CD80/His tag (10698-H08H), human B7-2/CD86/His tag (10699-H08H), human B7-DC/PD-L2/CD273/His tag (10292-H08H), human B7-H1/PD-L1/CD274/His tag (10084-H08H), human ICOS-L/B7-H2/His tag (11559-H08H), human B7-H4/B7S1/B7x/VCTN1/His tag (10738-H08H), human B7-H5/Gi24/VISTA/His tag (13482-H08H), human B7-H6/His tag (16140-H08H), human B7-H7(ECD)/HHLA2/Fc tag (16139-H02H), cynomolgus B7-H3(ECD)/Fc tag (90806-C02H), mB7-H3/His tag (50973-M08H), and m4-1BB/His tag (50811-M08H) (all from Sinobio). After washing with 0.05% Tween 20 in PBS and blocking with 1% bovine serum albumin (Gibco, 30063) in PBS, purified antibodies were added and incubated for 2 hours at 37°C. The wells were washed and incubated for 1 hour at 37°C with horseradish peroxidase (HRP)–conjugated goat anti-human IgG $F(ab')_2$ cross-adsorbed secondary antibody (Pierce, 31414) and developed with 3,3′,5,5′-tetramethylbenzidine

(Sigma-Aldrich, T0440). Absorbance at 450 nm was measured by SPECTROstar Nano (BMG Labtech).

SPR affinity assay was performed on a Biacore T200 (Cytiva). Anti–B7-H3 mAb was captured on Sensor Chip Protein A (Cytiva, 20127). Determination of hB7-H3 binding affinity was performed by applying dilutions of hB7-H3 protein (ranging from 3.125 to 100 nM) to the chip surface with a flow rate of 30 μl/min for 60 s; HBS-EP Buffer (Cytiva, BR100188) was passed over the surface for 180 s while monitoring hB7-H3 dissociation. Kinetics was analyzed under the 1:1 binding model (Langmuir model) by Biacore Insight Evaluation Software (Cytiva).

SDS–polyacrylamide gel electrophoresis

Purified 1D8, B5, and B5×1D8 were prepared in NuPAGE LDS sample buffer (Invitrogen, NP0007). For reducing samples, 2-mercaptoethanol (Sigma-Aldrich, M3148) was added in the sample buffer and heated at 70°C for 10 min. A total of 2.5 μg of each antibody and Novex Sharp Pre-stained Protein Standard (Invitrogen, LC5800) was loaded into the wells of NuPAGE 4-12% Bis-Tris Mini Protein Gel (Invitrogen, NP0321). After electrophoresis, the gel was stained by Imperial Protein Stain solution (Thermo Fisher Scientific, 24615).

Antibody labeling and ex vivo imaging

Purified 1D8, B5, and B5×1D8 were labeled with the VivoTag 680XL Protein Labeling Kit (PerkinElmer, NEV11118), according to the manufacturer's protocol. $MC38^{hB7\text{-}H3}$ cells were subcutaneously implanted into the 6-week-old female C57BL/6 mice. When tumor volume reached about 150 mm^3, mice were randomly allocated to different treatment groups (n = 3 to 4 per group) and intravenously injected with 680XL-labeled antibody solution in PBS. Twenty-four hours after intravenous injection, tumor tissue and spleen were prepared and imaged using a red channel of a Fluorescence In Vivo Imaging (FOBI) system (NeoScience), which were then analyzed using NEOimage software (NeoScience). The tumor/spleen ratio was calculated by dividing the mean values of the identified region of interests.

Therapeutic studies

4-1BB agonist monotherapy

For studies with a palpable model, 0.5×10^6 $MC38^{hB7\text{-}H3}$ or 0.1×10^6 $B16\text{-}F10^{hB7\text{-}H3}$ cells were subcutaneously implanted into the right flank of C57BL/6 and 4-1BB KO mice. $CT26^{hB7\text{-}H3}$ cells (0.5×10^6) were subcutaneously implanted into the right flank of BALB/c mice. Tumor growth was monitored by digital caliper measurements three times a week, and tumor volume was calculated with the following formula: length × width × width × 0.5, where length is the largest diameter and width is the smallest diameter. When the tumors reached 2 to 4 mm in diameter, usually 6 to 8 days after inoculation, mice were randomized to receive treatment. Tumor-bearing mice were treated with two (for MC38 and CT26 tumor model) or four (for B16-F10 tumor model) intraperitoneal injections (3-day interval) of InVivoPlus hIgG1 isotype control (Bio X Cell, BP0297), 1D8, B5, or B5×1D8. Four (for the B16-F10 tumor model) or 7 (for the MC38 and CT26 tumor model) days after the last treatment, serum was prepared to analyze the ALT/AST level. The dose of antibodies is determined by their molar ratio: mAb:bsAb = 3:4. Mice were euthanized when tumor size reached a diameter of 20.0 mm length. The tumor-free status was classified as a tumor with a diameter of less than 3 mm for three or more consecutive measurements. To study the immune memory responses, surviving mice from the $MC38^{hB7\text{-}H3}$ challenge and age-matched naïve mice were subcutaneously implanted with 0.5×10^6 parental MC38 tumor cells, which are not expressing hB7-H3, into the left flank. Some surviving mice were subcutaneously implanted with parental MC38 tumor cells on the left flank and irrelevant B16-F10 tumor cells on the right flank.

For studies with h4-1BB KI mice, 0.5×10^6 $MC38^{hB7\text{-}H3}$ cells were implanted into the right front flank. Tumor-bearing mice were randomly enrolled into treatment groups (n = 6 or 8 per group) when the mean tumor size reaches approximately 100 mm^3 (80 to 120 mm^3). Tumor-bearing mice were treated a total of five or six intraperitoneal injections (every 3 days) of hIgG1 isotype (7.5 mg/kg), B5 (7.5 mg/kg), 1A10 (7.5 mg/kg), or B5×1A10 (3 mg/kg) for Fig. 6D and hIgG1 isotype (2.25 mg/kg) or B5×1A10 (3 mg/kg) for Fig. 6E. Tumor growth was monitored twice a week, and mice were euthanized when tumor volume reached 3000 mm^3.

4-1BB agonist with ICB combination therapy

For the combination therapy, $MC38^{hB7\text{-}H3}$ tumor–bearing mice were randomized to receive the treatment when the tumor reached an average volume of 100 to 200 mm^3, usually 12 to 14 days after inoculation. Tumor-bearing mice were treated with four intraperitoneal injections (3-day interval) of hIgG1 isotype or B5×1D8 and two intraperitoneal injections (5-day interval) of InVivoMAb anti-mouse PD-1 (clone 29F.1A12), InVivoMAb anti-mouse CTLA-4 (clone 9D9), InVivoMAb anti-mouse Tim-3 (clone RMT3-23), or InVivoMAb rat IgG2a isotype control (clone 2A3) (all from Bio X Cell).

In vivo cell depletion

For a study with immune cell depletion, InVivoMAb anti-mouse CD4 (clone GK1.5), InVivoMAb anti-mouse CD8α (clone 2.43), InVivoMAb anti-mouse NK1.1 (clone PK136), and InVivoMAb rat IgG2b isotype control (clone LTF-2) (all from Bio X Cell) were intraperitoneally injected at −1, 1, 5, 8, and 11 days after the beginning of treatment at a dose of 0.2 mg per injection. The depletion efficiency was validated by flow cytometric analysis of peripheral blood.

Toxicity studies

Six-week-old female C57BL/6 mice received hIgG1 isotype (37.5 μg per injection), 1D8 (37.5 μg per injection), or B5×1D8 (50.0 μg per injection) once a week for 4 weeks. Seven days after the last treatment, mice were bled and sacrificed. Blood cells were analyzed with a VetScan HM2 hematology system (Abaxis). Mouse serum was obtained by centrifugation and stored at −80°C until analysis. Analysis of serum levels of ALT and AST was performed by KPC Lab Inc. or T&P Bio Co. Ltd. Tissues, including liver, spleen, and inguinal lymph node, were surgically removed and weighed, and single-cell suspensions were prepared for analyzing immune cell composition. BM cells were prepared into single cells for analyzing changes in the immune cell population.

Preparation of single cells from tumor tissue and tdLN

Tumor tissue and tdLN were harvested and weighed at 4 days after the last treatment in the $MC38^{hB7\text{-}H3}$ palpable tumor model. Tumor tissues were chopped and digested with 400 Mandl units of collagenase D (Roche, 11088882001) and deoxyribonuclease I (200 μg/ml; Roche, 11284932001) for 30 min at 37°C. Digested tumor tissues were dissociated into a single-cell suspension using a 100-μm cell strainer. tdLN was dissociated into a single-cell suspension using a

40-μm cell strainer. All single-cell suspensions are then maintained in the cIMDM for analysis.

Flow cytometry

Cell suspensions were washed and stained with Ghost Dye Violet 510 (Tonbo, 13-0870) in PBS according to the manufacturer's protocol. After live/dead staining, cells were incubated with Fc block (purified anti-mouse CD16/32 antibody, clone 93, BioLegend) and stained with indicated surface markers at 4°C for 20 min. For cytokine staining, cells were restimulated with phorbol 12-myristate 13-acetate (PMA; 20 ng/ml; Sigma-Aldrich, P8139) and ionomycin (1 μg/ml; Sigma-Aldrich, I0634) for 4 hours in the presence of GolgiStop (BD Biosciences, 554724) and GolgiPlug (BD Biosciences, 555029) followed by surface marker staining. Cells were then fixed and permeabilized with either Cytofix/Cytoperm solution (BD Biosciences) for cytokine staining or the Foxp3/Transcription factor staining buffer set (eBioscience) for GzmB, Ki-67, CTLA-4, and transcription factors according to the manufacturers' protocols. Cells were measured with BD LSRFortessa (BD Biosciences) or CytoFLEX LX (Beckman Coulter). Data were analyzed by FlowJo software (Treestar Inc.).

Antibodies (clone) used for the surface staining include CD4 (RM4-5), CD8α (53-6.7), CD11b (M1/70), CD11c (N418), CD19 (1D3), CD25 (PC61.5), CD44 (IM7), CD45 (30-F11), CD62L (MEL-14), CD137/4-1BB (17B5), CD223/LAG-3 (C9B7W), CD276/B7-H3 (EPNCIR122), CD279/PD-1 (RMP1-30), CD335/NKp46 (29A1.4), CD366/Tim-3 (RMT3-23), NK1.1 (PK136), Slamf6 (13G3), TCR-β (H57-597), rat anti-mouse IgG1 (A85-1), mouse anti-human IgG Fc (HP6017), goat anti-rabbit IgG H&L, and anti–hB7-H3 (185504). Antibodies (clone) used for the intracellular staining include CD152/CTLA-4 (UC10-4B9), Eomes (Dan11mag), Foxp3 (FJK-16 s), GzmB (GB11), IFN-γ (XMG1.2), Ki-67 (SolA15), T-bet (4B10), TCF1/TCF7 (C63D9), and TNF-α (MP6-XT212). All antibodies were purchased from BioLegend, eBioscience, BD Biosciences, R&D Systems, Abcam, or Cell Signaling Technology.

Tumor tissue lysis and cytokine ELISA

Tumor tissue was harvested and sonicated in the presence of radioimmunoprecipitation assay buffer (Sigma-Aldrich, R0278). After sonication, lysates were prepared by centrifugation, and protein concentration was then measured using the Pierce BCA Protein Assay Kit (Thermo Fisher Scientific, 23227) according to the manufacturer's protocol. IFN-γ and TNF-α levels in the tumor lysates were measured using a mouse IFN-γ DuoSet ELISA kit (R&D Systems, DY485) and a mouse TNF-α DuoSet ELISA kit (R&D Systems, DY410), respectively.

h4-1BB signaling reporter assay

B7-H3–expressing (MCF-7, HCC1954, MDA-MB-231, and PANC-1) or nonexpressing (KATO III) cancer cells (2.5×10^4) were seeded in a 96-well plate and incubated overnight in a CO_2 incubator at 37°C. The next day, 2.5×10^4 GloResponse NFκB-Luc2/h4-1BB Jurkat cells (Promega, CS196004) in assay medium (RPMI 1640 + 1% FBS) were added with the 4-1BB agonist. 1A10 mAb was incubated for 15 min with an anti-human IgG Fc secondary antibody (Thermo Fisher Scientific, 31125) to induce cross-linking. Six hours after culture, an equal volume of Bio-Glo luciferase assay reagent (Promega, G7940) was added, and luciferase activity was analyzed by measuring luminescence using a PHERAstar FSX microplate reader (BMG Labtech).

Human PBMC activation and target cell lysis assay

LEAF purified anti-human CD3 antibody (clone UCHT1, BioLegend, 300438) was immobilized (5 μg/ml) on an assay plate overnight at 4°C. After removal of unbound anti-human CD3 antibody, uncharacterized PBMC (C.T.L., CTL-UP1, lot no. HHU20180509) effector cells (3×10^4 cells per well), indicated doses of purified antibodies, and HCC1954 target cells (1×10^4 cells per well) were added and incubated for 72 hours at 37°C in a humidified incubator with 5% CO_2. Supernatants were collected and assayed for IFN-γ secretion using a human IFN-γ Quantikine ELISA kit (R&D Systems, SIF50). Cell viability was analyzed by measuring absorbance at 450 nm after adding cell counting kit-8 (Dojindo, CK04-20) according to the manufacturer's protocol.

Pharmacokinetics

Antibodies (B5 or B5×1A10) (10 mg/kg) were administered to naïve mice intravenously, and then serum was collected at 0.05, 3, 8, 24, 48, 96, 168, 240, 336, 432, 528, and 624 hours after administration. The serum concentration of antibodies was measured by ELISA against hB7-H3 protein with HRP-conjugated goat anti-human IgG $F(ab')_2$.

Immunohistochemistry

Tumor tissues were fixed with formalin, embedded in paraffin blocks, and cut into 4-μm-thick sections. Following deparaffinization and rehydration, the sections underwent heat antigen retrieval in tris-EDTA buffer (pH 9.0). Sections were blocked for 10% normal goat serum and stained with anti-mouse CD8 (Abcam, ab209775) using VECTASTAIN Elite ABC kits (VECTOR Laboratories, PK-6101). The tissues were subsequently developed using a DAB substrate kit (VECTOR Laboratories, SK-4100) and counterstained with Mayer's hematoxylin (Dako, S330930). Slides were mounted and imaged using a ZEISS Axio Observer Z1 microscope. For the quantification of $CD8^+$ TILs, slides were digitally scanned at ×400 magnification using a MoticEasyScan One scanner (Motic). The number of $CD8^+$ cells was evaluated as the average of randomly selected areas within the tumor-infiltrative area of each slide.

Statistical analysis

Statistical analysis was performed using GraphPad Prism Software version 8.4. All the in vitro experiments were done in duplicate or triplicate, and values were presented as means ± SD from one of the independent experiment sets. EC_{50} values were determined using a nonlinear regression curve. Tumor growth curves were shown as means with SEM. The statistical tests used were indicated in the figure legends for each experiment. In the tumor growth curves, only P values on the last day were shown. Asterisks indicated P values as $^*P < 0.05$; $^{**}P < 0.01$; $^{***}P < 0.001$; $^{****}P < 0.0001$.

SUPPLEMENTARY MATERIALS

Supplementary material for this article is available at http://advances.sciencemag.org/cgi/content/full/7/3/eaax3160/DC1

View/request a protocol for this paper from *Bio-protocol*.

REFERENCES AND NOTES

1. J. G. Egen, W. Ouyang, L. C. Wu, Human anti-tumor immunity: Insights from immunotherapy clinical trials. *Immunity* **52**, 36–54 (2020).
2. L. L. Siu, S. P. Ivy, E. L. Dixon, A. E. Gravell, S. A. Reeves, G. L. Rosner, Challenges and opportunities in adapting clinical trial design for immunotherapies. *Clin. Cancer Res.* **23**, 4950–4958 (2017).

3. A. Ribas, J. D. Wolchok, Cancer immunotherapy using checkpoint blockade. *Science* **359**, 1350–1355 (2018).
4. A. Wyzgol, N. Müller, A. Fick, S. Munkel, G. U. Grigoleit, K. Pfizenmaier, H. Wajant, Trimer stabilization, oligomerization, and antibody-mediated cell surface immobilization improve the activity of soluble trimers of CD27L, CD40L, 41BBL, and glucocorticoid-induced TNF receptor ligand. *J. Immunol.* **183**, 1851–1861 (2009).
5. T. So, S.-W. Lee, M. Croft, Tumor necrosis factor/tumor necrosis factor receptor family members that positively regulate immunity. *Int. J. Hematol.* **83**, 1–11 (2006).
6. S. Jeong, S.-H. Park, Co-stimulatory receptors in cancers and their implications for cancer immunotherapy. *Immune Netw.* **20**, e3 (2020).
7. C. Chester, M. F. Sanmamed, J. Wang, I. Melero, Immunotherapy targeting 4-1BB: Mechanistic rationale, clinical results, and future strategies. *Blood* **131**, 49–57 (2018).
8. L. M. Myers, A. T. Vella, Interfacing T-cell effector and regulatory function through CD137 (4-1BB) co-stimulation. *Trends Immunol.* **26**, 440–446 (2005).
9. Q. Ye, D. G. Song, M. Poussin, T. Yamamoto, A. Best, C. Li, G. Coukos, D. J. Powell, CD137 accurately identifies and enriches for naturally occurring tumor-reactive T cells in tumor. *Clin. Cancer Res.* **20**, 44–55 (2014).
10. J. B. Williams, B. L. Horton, Y. Zheng, Y. Duan, J. D. Powell, T. F. Gajewski, The EGR2 targets LAG-3 and 4-1BB describe and regulate dysfunctional antigen-specific CD8$^+$ T cells in the tumor microenvironment. *J. Exp. Med.* **214**, 381–400 (2017).
11. I. Melero, W. W. Shuford, S. A. Newby, A. Aruffo, J. A. Ledbetter, K. E. Hellström, R. S. Mittler, L. Chen, Monoclonal antibodies against the 4-1BB T-cell activation molecule eradicate established tumors. *Nat. Med.* **3**, 682–685 (1997).
12. N. H. Segal, T. F. Logan, F. S. Hodi, D. McDermott, I. Melero, O. Hamid, H. Schmidt, C. Robert, V. Chiarion-Sileni, P. A. Ascierto, M. Maio, W. J. Urba, T. C. Gangadhar, S. Suryawanshi, J. Neely, M. Jure-Kunkel, S. Krishnan, H. Kohrt, M. Sznol, R. Levy, Results from an integrated safety analysis of urelumab, an agonist anti-CD137 monoclonal antibody. *Clin. Cancer Res.* **23**, 1929–1936 (2017).
13. L. Niu, S. Strahotin, B. Hewes, B. Zhang, Y. Zhang, D. Archer, T. Spencer, D. Dillehay, B. Kwon, L. Chen, A. T. Vella, R. S. Mittler, Cytokine-mediated disruption of lymphocyte trafficking, hemopoiesis, and induction of lymphopenia, anemia, and thrombocytopenia in anti-CD137-treated mice. *J. Immunol.* **178**, 4194–4213 (2007).
14. J. Dubrot, F. Milheiro, C. Alfaro, A. Palazón, I. Martinez-Forero, J. L. Perez-Gracia, A. Morales-Kastresana, J. L. Romero-Trevejo, M. C. Ochoa, S. Hervás-Stubbs, J. Prieto, M. Jure-Kunkel, L. Chen, I. Melero, Treatment with anti-CD137 mAbs causes intense accumulations of liver T cells without selective antitumor immunotherapeutic effects in this organ. *Cancer Immunol. Immunother.* **59**, 1223–1233 (2010).
15. S.-W. Lee, S. Salek-Ardakani, R. S. Mittler, M. Croft, Hypercostimulation through 4-1BB distorts homeostasis of immune cells. *J. Immunol.* **182**, 6753–6762 (2009).
16. X. Qi, F. Li, Y. Wu, C. Cheng, P. Han, J. Wang, X. Yang, Optimization of 4-1BB antibody for cancer immunotherapy by balancing agonistic strength with FcγR affinity. *Nat. Commun.* **10**, 2141 (2019).
17. M. Compte, S. L. Harwood, I. G. Muñoz, R. Navarro, M. Zonca, G. Perez-Chacon, A. Erce-Llamazares, N. Merino, A. Tapia-Galisteo, A. M. Cuesta, K. Mikkelsen, E. Caleiras, N. Nuñez-Prado, M. A. Aznar, S. Lykkemark, J. Martínez-Torrecuadrada, I. Melero, F. J. Blanco, J. Bernardino de la Serna, J. M. Zapata, L. Sanz, L. Alvarez-Vallina, A tumor-targeted trimeric 4-1BB-agonistic antibody induces potent anti-tumor immunity without systemic toxicity. *Nat. Commun.* **9**, 4809 (2018).
18. C. Claus, C. Ferrara, W. Xu, J. Sam, S. Lang, F. Uhlenbrock, R. Albrecht, S. Herter, R. Schlenker, T. Hüsser, S. Diggelmann, J. Challier, E. Mössner, R. J. Hosse, T. Hofer, P. Brünker, C. Joseph, J. Benz, P. Ringler, H. Stahlberg, M. Lauer, M. Perro, S. Chen, C. Küttel, P. L. Bhavani Mohan, V. Nicolini, M. C. Birk, A. Ongaro, C. Prince, R. Gianotti, G. Dugan, C. T. Whitlow, K. K. Solingapuram Sai, D. L. Caudell, A. G. Burgos-Rodriguez, J. M. Cline, M. Hettich, M. Ceppi, A. M. Giusti, F. Crameri, W. Driessen, P. N. Morcos, A. Freimoser-Grundschober, V. Levitsky, M. Amann, S. Grau-Richards, T. von Hirschheydt, S. Tournaviti, M. Mølhøj, T. Fauti, V. Heinzelmann-Schwarz, V. Teichgräber, S. Colombetti, M. Bacac, A. Zippelius, C. Klein, P. Umaña, Tumor-targeted 4-1BB agonists for combination with T cell bispecific antibodies as off-the-shelf therapy. *Sci. Transl. Med.* **11**, eaav5989 (2019).
19. M. J. Hinner, R. S. B. Aiba, T. J. Jaquin, S. Berger, M. C. Dürr, C. Schlosser, A. Allersdorfer, A. Wiedenmann, G. Matschiner, J. Schüler, U. Moebius, C. Rothe, L. Matis, S. A. Olwill, Tumor-localized costimulatory T-cell engagement by the 4-1BB/HER2 bispecific antibody-anticalin fusion PRS-343. *Clin. Cancer Res.* **25**, 5878–5889 (2019).
20. S. J. Im, M. Hashimoto, M. Y. Gerner, J. Lee, H. T. Kissick, M. C. Burger, Q. Shan, J. S. Hale, J. Lee, T. H. Nasti, A. H. Sharpe, G. J. Freeman, R. N. Germain, H. I. Nakaya, H. H. Xue, R. Ahmed, Defining CD8$^+$ T cells that provide the proliferative burst after PD-1 therapy. *Nature* **537**, 417–421 (2016).
21. B. C. Miller, D. R. Sen, R. al Abosy, K. Bi, Y. V. Virkud, M. W. LaFleur, K. B. Yates, A. Lako, K. Felt, G. S. Naik, M. Manos, E. Gjini, J. R. Kuchroo, J. J. Ishizuka, J. L. Collier, G. K. Griffin, S. Maleri, D. E. Comstock, S. A. Weiss, F. D. Brown, A. Panda, M. D. Zimmer, R. T. Manguso, F. S. Hodi, S. J. Rodig, A. H. Sharpe, W. N. Haining, Subsets of exhausted CD8$^+$ T cells differentially mediate tumor control and respond to checkpoint blockade. *Nat. Immunol.* **20**, 326–336 (2019).
22. J. Brummelman, E. M. C. Mazza, G. Alvisi, F. S. Colombo, A. Grilli, J. Mikulak, D. Mavilio, M. Alloisio, F. Ferrari, E. Lopci, P. Novellis, G. Veronesi, E. Lugli, High-dimensional single cell analysis identifies stem-like cytotoxic CD8$^+$ T cells infiltrating human tumors. *J. Exp. Med.* **215**, 2520–2535 (2018).
23. I. Siddiqui, K. Schaeuble, V. Chennupati, S. A. Fuertes Marraco, S. Calderon-Copete, D. P. Ferreira, S. J. Carmona, L. Scarpellino, D. Gfeller, S. Pradervand, S. A. Luther, D. E. Speiser, W. Held, Intratumoral Tcf1$^+$PD-1$^+$CD8$^+$ T cells with stem-like properties promote tumor control in response to vaccination and checkpoint blockade immunotherapy. *Immunity* **50**, 195–211.e10 (2019).
24. D. T. Utzschneider, M. Charmoy, V. Chennupati, L. Pousse, D. P. Ferreira, S. Calderon-Copete, M. Danilo, F. Alfei, M. Hofmann, D. Wieland, S. Pradervand, R. Thimme, D. Zehn, W. Held, T cell factor 1-expressing memory-like CD8$^+$ T cells sustain the immune response to chronic viral infections. *Immunity* **45**, 415–427 (2016).
25. C. S. Jansen, N. Prokhnevska, V. A. Master, M. G. Sanda, J. W. Carlisle, M. A. Bilen, M. Cardenas, S. Wilkinson, R. Lake, A. G. Sowalsky, R. M. Valanparambil, W. H. Hudson, D. McGuire, K. Melnick, A. I. Khan, K. Kim, Y. M. Chang, A. Kim, C. P. Filson, M. Alemozaffar, A. O. Osunkoya, P. Mullane, C. Ellis, R. Akondy, S. J. Im, A. O. Kamphorst, A. Reyes, Y. Liu, H. Kissick, An intra-tumoral niche maintains and differentiates stem-like CD8 T cells. *Nature* **576**, 465–470 (2019).
26. W. H. Hudson, J. Gensheimer, M. Hashimoto, A. Wieland, R. M. Valanparambil, P. Li, J.-X. Lin, B. T. Konieczny, S. J. Im, G. J. Freeman, W. J. Leonard, H. T. Kissick, R. Ahmed, Proliferating transitory T cells with an effector-like transcriptional signature emerge from PD-1$^+$ stem-like CD8$^+$ T cells during chronic infection. *Immunity* **51**, 1043–1058.e4 (2019).
27. G. P. Mognol, R. Spreafico, V. Wong, J. P. Scott-Browne, S. Togher, A. Hoffmann, P. G. Hogan, A. Rao, S. Trifari, Exhaustion-associated regulatory regions in CD8$^+$ tumor-infiltrating T cells. *Proc. Natl. Acad. Sci. U.S.A.* **114**, E2776–E2785 (2017).
28. E. Picarda, K. C. Ohaegbulam, X. Zang, Molecular pathways: Targeting B7-H3 (CD276) for human cancer immunotherapy. *Clin. Cancer Res.* **22**, 3425–3431 (2016).
29. S. Seaman, Z. Zhu, S. Saha, X. M. Zhang, M. Y. Yang, M. B. Hilton, K. Morris, C. Szot, H. Morris, D. A. Swing, L. Tessarollo, S. W. Smith, S. Degrado, D. Borkin, N. Jain, J. Scheiermann, Y. Feng, Y. Wang, J. Li, D. Welsch, G. De Crescenzo, A. Chaudhary, E. Zudaire, K. D. Klarmann, J. R. Keller, D. S. Dimitrov, B. St. Croix, Eradication of tumors through simultaneous ablation of CD276/B7-H3-positive tumor cells and tumor vasculature. *Cancer Cell* **31**, 501–515.e8 (2017).
30. W. W. Shuford, K. Klussman, D. D. Tritchler, D. T. Loo, J. Chalupny, A. W. Siadak, T. J. Brown, J. Emswiler, H. Raecho, C. P. Larsen, T. C. Pearson, J. A. Ledbetter, A. Aruffo, R. S. Mittler, 4-1BB costimulatory signals preferentially induce CD8$^+$ T cell proliferation and lead to the amplification in vivo of cytotoxic T cell responses. *J. Exp. Med.* **186**, 47–55 (1997).
31. R. L. Shields, A. K. Namenuk, K. Hong, Y. G. Meng, J. Rae, J. Briggs, D. Xie, J. Lai, A. Stadlen, B. Li, J. A. Fox, L. G. Presta, High resolution mapping of the binding site on human IgG1 for FcγRI, FcγRII, FcγRIII, and FcRn and design of IgG1 variants with improved binding to the FcγR. *J. Biol. Chem.* **276**, 6591–6604 (2001).
32. S.-A. Ju, S.-M. Park, S.-C. Lee, B. S. Kwon, B.-S. Kim, Marked expansion of CD11c+CD8+ T-cells in melanoma-bearing mice induced by anti-4-1BB monoclonal antibody. *Mol. Cells* **24**, 132–138 (2007).
33. W. Zhong, J. S. Myers, F. Wang, K. Wang, J. Lucas, E. Rosfjord, J. Lucas, A. T. Hooper, S. Yang, L. A. Lemon, M. Guffroy, C. May, J. R. Bienkowska, P. A. Rejto, Comparison of the molecular and cellular phenotypes of common mouse syngeneic models with human tumors. *BMC Genomics* **21**, 2 (2020).
34. R. A. Wilcox, D. B. Flies, G. Zhu, A. J. Johnson, K. Tamada, A. I. Chapoval, S. E. Strome, L. R. Pease, L. Chen, Provision of antigen and CD137 signaling breaks immunological ignorance, promoting regression of poorly immunogenic tumors. *J. Clin. Invest.* **109**, 651–659 (2002).
35. R. Houot, M. J. Goldstein, H. E. Kohrt, J. H. Myklebust, A. A. Alizadeh, J. T. Lin, J. M. Irish, J. A. Torchia, A. Kolstad, L. Chen, R. Levy, Therapeutic effect of CD137 immunomodulation in lymphoma and its enhancement by Treg depletion. *Blood* **114**, 3431–3438 (2009).
36. E. Kocak, K. Lute, X. Chang, K. F. May Jr., K. R. Exten, H. Zhang, S. F. Abdessalam, A. M. Lehman, D. Jarjoura, P. Zheng, Y. Liu, Combination therapy with anti–CTL antigen-4 and anti-4-1BB antibodies enhances cancer immunity and reduces autoimmunity. *Cancer Res.* **66**, 7276–7284 (2006).
37. Y. Ohue, H. Nishikawa, Regulatory T (Treg) cells in cancer: Can Treg cells be a new therapeutic target? *Cancer Sci.* **110**, 2080–2089 (2019).
38. S. M. Kahan, A. J. Zajac, Immune exhaustion: Past lessons and new insights from lymphocytic choriomeningitis virus. *Viruses* **11**, 156 (2019).
39. K. E. Pauken, E. J. Wherry, Overcoming T cell exhaustion in infection and cancer. *Trends Immunol.* **36**, 265–276 (2015).
40. M. A. Curran, T. L. Geiger, W. Montalvo, M. Kim, S. L. Reiner, A. al-Shamkhani, J. C. Sun, J. P. Allison, Systemic 4-1BB activation induces a novel T cell phenotype driven by high expression of Eomesodermin. *J. Exp. Med.* **210**, 743–755 (2013).
41. S. Chen, L.-F. Lee, T. S. Fisher, B. Jessen, M. Elliott, W. Evering, K. Logronio, G. H. Tu, K. Tsaparikos, X. Li, H. Wang, C. Ying, M. Xiong, T. VanArsdale, J. C. Lin, Combination

of 4-1BB agonist and PD-1 antagonist promotes antitumor effector/memory CD8 T cells in a poorly immunogenic tumor model. *Cancer Immunol. Res.* **3**, 149–160 (2015).
42. H. Wei, L. Zhao, I. Hellstrom, K. E. Hellstrom, Y. Guo, Dual targeting of CD137 co-stimulatory and PD-1 co-inhibitory molecules for ovarian cancer immunotherapy. *Oncoimmunology* **3**, e28248 (2014).
43. Y. Shindo, K. Yoshimura, A. Kuramasu, Y. Watanabe, H. Ito, T. Kondo, A. Oga, H. Ito, S. Yoshino, S. Hazama, K. Tamada, H. Yagita, M. Oka, Combination immunotherapy with 4-1BB activation and PD-1 blockade enhances antitumor efficacy in a mouse model of subcutaneous tumor. *Anticancer Res.* **35**, 129–136 (2015).
44. M. A. Curran, M. Kim, W. Montalvo, A. Al-Shamkhani, J. P. Allison, Combination CTLA-4 blockade and 4-1BB activation enhances tumor rejection by increasing T-cell infiltration, proliferation, and cytokine production. *PLOS ONE* **6**, e19499 (2011).
45. Z. Guo, D. Cheng, Z. Xia, M. Luan, L. Wu, G. Wang, S. Zhang, Combined TIM-3 blockade and CD137 activation affords the long-term protection in a murine model of ovarian cancer. *J. Transl. Med.* **11**, 215 (2013).
46. S. M. Chin, C. R. Kimberlin, Z. Roe-Zurz, P. Zhang, A. Xu, S. Liao-Chan, D. Sen, A. R. Nager, N. S. Oakdale, C. Brown, F. Wang, Y. Yang, K. Lindquist, Y. A. Yeung, S. Salek-Ardakani, J. Chaparro-Riggers, Structure of the 4-1BB/4-1BBL complex and distinct binding and functional properties of utomilumab and urelumab. *Nat. Commun.* **9**, 4679 (2018).
47. J. Theruvath, E. Sotillo, C. W. Mount, C. M. Graef, A. Delaidelli, S. Heitzeneder, L. Labanieh, S. Dhingra, A. Leruste, R. G. Majzner, P. Xu, S. Mueller, D. W. Yecies, M. A. Finetti, D. Williamson, P. D. Johann, M. Kool, S. Pfister, M. Hasselblatt, M. C. Frühwald, O. Delattre, D. Surdez, F. Bourdeaut, S. Puget, S. Zaidi, S. S. Mitra, S. Cheshier, P. H. Sorensen, M. Monje, C. L. Mackall, Locoregionally administered B7-H3-targeted CAR T cells for treatment of atypical teratoid/rhabdoid tumors. *Nat. Med.* **26**, 712–719 (2020).
48. X. Qin, H. Zhang, D. Ye, B. Dai, Y. Zhu, G. Shi, B7-H3 is a new cancer-specific endothelial marker in clear cell renal cell carcinoma. *Onco Targets Ther.* **6**, 1667–1673 (2013).
49. X. Zang, R. H. Thompson, H. A. al-Ahmadie, A. M. Serio, V. E. Reuter, J. A. Eastham, P. T. Scardino, P. Sharma, J. P. Allison, B7-H3 and B7x are highly expressed in human prostate cancer and associated with disease spread and poor outcome. *Proc. Natl. Acad. Sci. U.S.A.* **104**, 19458–19463 (2007).
50. K. A. Hofmeyer, A. Ray, X. Zang, The contrasting role of B7-H3. *Proc. Natl. Acad. Sci. U.S.A.* **105**, 10277–10278 (2008).
51. K. Yonesaka, K. Haratani, S. Takamura, H. Sakai, R. Kato, N. Takegawa, T. Takahama, K. Tanaka, H. Hayashi, M. Takeda, S. Kato, O. Maenishi, K. Sakai, Y. Chiba, T. Okabe, K. Kudo, Y. Hasegawa, H. Kaneda, M. Yamato, K. Hirotani, M. Miyazawa, K. Nishio, K. Nakagawa, B7-H3 negatively modulates CTL-mediated cancer immunity. *Clin. Cancer Res.* **24**, 2653–2664 (2018).
52. W.-K. Suh, B. U. Gajewska, H. Okada, M. A. Gronski, E. M. Bertram, W. Dawicki, G. S. Duncan, J. Bukczynski, S. Plyte, A. Elia, A. Wakeham, A. Itie, S. Chung, J. da Costa, S. Arya, T. Horan, P. Campbell, K. Gaida, P. S. Ohashi, T. H. Watts, S. K. Yoshinaga, M. R. Bray, M. Jordana, T. W. Mak, The B7 family member B7-H3 preferentially down-regulates T helper type 1–mediated immune responses. *Nat. Immunol.* **4**, 899–906 (2003).
53. Y.-H. Lee, N. Martin-Orozco, P. Zheng, J. Li, P. Zhang, H. Tan, H. J. Park, M. Jeong, S. H. Chang, B.-S. Kim, W. Xiong, W. Zang, L. Guo, Y. Liu, Z.-J. Dong, W. W. Overwijk, P. Hwu, Q. Yi, L. Kwak, Z. Yang, T. W. Mak, W. Li, L. G. Radvanyi, L. Ni, D. Liu, C. Dong, Inhibition of the B7-H3 immune checkpoint limits tumor growth by enhancing cytotoxic lymphocyte function. *Cell Res.* **27**, 1034–1045 (2017).
54. J. Ma, B. Zheng, S. Goswami, L. Meng, D. Zhang, C. Cao, T. Li, F. Zhu, L. Ma, Z. Zhang, S. Zhang, M. Duan, Q. Chen, Q. Gao, X. Zhang, PD1^{Hi} CD8^{+} T cells correlate with exhausted signature and poor clinical outcome in hepatocellular carcinoma. *J. Immunother. Cancer* **7**, 331 (2019).
55. I. J. Datar, M. F. Sanmamed, J. Wang, B. S. Henick, J. Choi, T. Badri, W. Dong, N. Mani, M. Toki, L. D. Mejías, M. D. Lozano, J. L. Perez-Gracia, V. Velcheti, M. D. Hellmann, J. F. Gainor, K. M. Eachern, D. Jenkins, K. Syrigos, K. Politi, S. Gettinger, D. L. Rimm, R. S. Herbst, I. Melero, L. Chen, K. A. Schalper, Expression analysis and significance of PD-1, LAG-3 and TIM-3 in human non-small cell lung cancer using spatially-resolved and multiparametric single-cell analysis. *Clin. Cancer Res.* **25**, 4663–4673 (2019).
56. H.-D. Kim, S. Park, S. Jeong, Y. J. Lee, H. Lee, C. G. Kim, K. H. Kim, S.-M. Hong, J.-Y. Lee, S. Kim, H. K. Kim, B. S. Min, J. H. Chang, Y. S. Ju, E.-C. Shin, G.-W. Song, S. Hwang, S.-H. Park, 4-1BB delineates distinct activation status of exhausted tumor-infiltrating CD8^{+} T cells in hepatocellular carcinoma. *Hepatology* **71**, 955–971 (2020).

Acknowledgments: We thank S. A. Lim and M. O. Lee for excellent technical assistance.
Funding: This work was supported by the BK21 funded by the Ministry of Education, Republic of Korea (4120200313623), by the Bio & Medical Technology Development Program of the National Research Foundation (NRF) funded by the Korean government (MSIT) (NRF-2020M3H1A1075314), and by grants from ABL Bio Inc., Korea and Dong-A ST Co. Ltd., Korea.
Author contributions: G.Y., Y.L., J.W., J.J., and S.-W.L. conceived the study and designed experiments. K.P. and W.S. performed antibody production. G.Y., Y.-W.K., K.P., W.S., H.C., U.-j.J., and Y.-G.S. performed the in vitro experiment. G.Y., Y.-W.K., H.W.P., H.K., Y.-M.K., S.K., J.-H.K., and D.M. performed animal experiments. E.P. designed h4-1BB KI mice experiments. S.L. performed immunohistochemical imaging. J.E. performed pharmacokinetics analysis. G.Y., Y.L., J.W., J.J., and S.-W.L. analyzed data and wrote the manuscript. G.Y., Y.L., J.W., Y.P., J.J., and S.-W.L. edited the manuscript. All authors have discussed the results and provided comments on the manuscript for improving the manuscript. **Competing interests:** Y.L., K.P., H.C., W.S., U.-j.J., E.P., S.L., Y.-G.S., J.E., J.W., and J.J. are employees of ABL Bio Inc., which develops and supports the supply of recombinant antibodies presented in this manuscript. The other authors declare no potential competing interests. **Data and materials availability:** All data needed to evaluate the conclusions in the paper are present in the paper and/or the Supplementary Materials. Additional data related to this paper may be requested from the authors.

Submitted 27 May 2020
Accepted 19 November 2020
Published 15 January 2021
10.1126/sciadv.aax3160

Citation: G. You, Y. Lee, Y.-W. Kang, H. W. Park, K. Park, H. Kim, Y.-M. Kim, S. Kim, J.-H. Kim, D. Moon, H. Chung, W. Son, U.-j. Jung, E. Park, S. Lee, Y.-G. Son, J. Eom, J. Won, Y. Park, J. Jung, S.-W. Lee, B7-H3×4-1BB bispecific antibody augments antitumor immunity by enhancing terminally differentiated CD8^{+} tumor-infiltrating lymphocytes. *Sci. Adv.* **7**, eaax3160 (2021).

Science Advances

B7-H3×4-1BB bispecific antibody augments antitumor immunity by enhancing terminally differentiated CD8 $^{+}$ tumor-infiltrating lymphocytes

Gihoon You, Yangsoon Lee, Yeon-Woo Kang, Han Wook Park, Kyeongsu Park, Hyekang Kim, Young-Min Kim, Sora Kim, Ji-Hae Kim, Dain Moon, Hyejin Chung, Wonjun Son, Ui-jung Jung, Eunyoung Park, Shinai Lee, Yong-Gyu Son, Jaehyun Eom, Jonghwa Won, Yunji Park, Jaeho Jung and Seung-Woo Lee

Sci Adv **7** (3), eaax3160.
DOI: 10.1126/sciadv.aax3160